

Enhancing Sensitivity to Leptonic CP Violation using Complementarity among DUNE, T2HK, and T2HKK

Sanjib Kumar Agarwalla,^{a,b,c,d} Sudipta Das,^{a,b} Alessio Giarnetti,^e Davide Meloni,^e
Masoom Singh^{a,f}

^a*Institute of Physics, Sachivalaya Marg, Sainik School Post, Bhubaneswar 751005, India*

^b*Homi Bhabha National Institute, Training School Complex, Anushakti Nagar, Mumbai 400094, India*

^c*International Centre for Theoretical Physics, Strada Costiera 11, 34151 Trieste, Italy*

^d*Department of Physics & Wisconsin IceCube Particle Astrophysics Center, University of Wisconsin, Madison, WI 53706, U.S.A*

^e*Dipartimento di Matematica e Fisica, Università di Roma Tre Via della Vasca Navale 84, 00146 Rome, Italy*

^f*Department of Physics, Utkal University, Vani Vihar, Bhubaneswar 751004, India*

E-mail: sanjib@iopb.res.in (ORCID:0000-0002-9714-8866),
sudipta.d@iopb.res.in (ORCID:0000-0002-5508-7751),
giarnetti.alessio@uniroma3.it (ORCID:0000-0001-8487-8045),
davide.meloni@uniroma3.it (ORCID:0000-0001-7680-6957),
masoom@iopb.res.in (ORCID:0000-0002-8363-7693)

ABSTRACT: After the landmark discovery of non-zero θ_{13} by the modern reactor experiments, unprecedented precision on neutrino mass-mixing parameters has been achieved over the past decade. This has set the stage for the discovery of leptonic CP violation (LCPV) at high confidence level in the next-generation long-baseline neutrino oscillation experiments. In this work, we explore in detail the possible complementarity among the on-axis DUNE and off-axis T2HK experiments to enhance the sensitivity to LCPV suppressing the $\theta_{23} - \delta_{\text{CP}}$ degeneracy. We find that none of these experiments individually can achieve the milestone of 3σ LCPV for at least 75% choices of δ_{CP} in its entire range of $[-180^\circ, 180^\circ]$, with their nominal exposures and systematic uncertainties. However, their combination can attain the same for all values of θ_{23} with only half of their nominal exposures. We observe that the proposed T2HKK setup in combination with DUNE can further increase the CP coverage to more than 80% with only half of their nominal exposures. We study in detail how the coverage in δ_{CP} for $\geq 3\sigma$ LCPV depends on the choice of θ_{23} , exposure, optimal runtime in neutrino and antineutrino modes, and systematic uncertainties in these experiments in isolation and combination. We find that with an improved systematic uncertainty of 2.7% in appearance mode, the standalone T2HK setup can provide a CP coverage of around 75% for all values of θ_{23} . We also discuss the pivotal role of intrinsic, extrinsic, and total CP asymmetries in the appearance channel and extrinsic CP asymmetries in the disappearance channel while analyzing our results.

KEYWORDS: Neutrino, Oscillation, Long-Baseline, CP Violation, DUNE, T2HK, T2HKK

ARXIV EPRINT: [2111.aaaaa](https://arxiv.org/abs/2111.aaaaa)

Contents

1	Introduction and Motivation	1
2	Discussion at the Oscillation Probability Level	4
2.1	Extrinsic, Intrinsic, and Total CP Asymmetries in Appearance Channel	5
2.2	Extrinsic CP Asymmetry in Disappearance Channel	8
2.3	$\theta_{23} - \delta_{\text{CP}}$ Degeneracy	10
3	Experimental Features and Simulation Details	12
4	Our Results	14
4.1	Impact of θ_{23} on CP coverage	15
4.2	CP coverage as a function of Exposure	18
4.3	Optimizing Runtime for maximal CP coverage	19
4.4	Impact of Systematic Uncertainties on CP coverage	20
4.5	Effect of Current 3σ Allowed Range in δ_{CP} on CP coverage	21
5	Summary and Conclusions	23

1 Introduction and Motivation

One of the fundamental properties of particles is their behavior under the CP (charge-parity) transformation and a violation of the CP symmetry may have an important connection to the observed baryon asymmetry in the Universe [1]. So far, in the quark sector of the Standard Model (SM), we have two known sources of CP-invariance violation [2]. One of them is the CP-odd phase in the Cabibbo-Kobayashi-Maskawa (CKM) matrix, which is known to be large and governs all the CP-violating phenomena observed so far. The other one is the so-called strong CP-phase θ_{QCD} , which is known to be vanishingly small. In the lepton sector, we achieved an important breakthrough in 2012 in establishing the standard three-flavor oscillation picture of neutrinos through the pioneering discovery of the non-zero value of the smallest neutral lepton mixing angle θ_{13} by the Daya Bay reactor antineutrino experiment [3]. This landmark finding opened the door for a completely new and independent source of CP invariance violation in neutrino oscillation experiments. The so-called Dirac CP-odd phase δ_{CP} in the 3×3 unitary Pontecorvo-Maki-Nakagawa-Sakata (PMNS) matrix is the source of CP-invariance violation in the neutral lepton sector, which can be probed via neutrino oscillation probabilities.

After the discovery of non-zero θ_{13} , remarkable precision has been achieved on neutrino mass-mixing parameters over the past decade, which has enabled us to come up with a simple, robust, three-flavor neutrino oscillation paradigm, which is capable to accommodate

most of the oscillation data [4–7]. In 3ν oscillation picture, if the value of δ_{CP} turns out to be different from both 0° and 180° in Nature, then it would cause a difference between neutrino and antineutrino transition probabilities – providing a smoking gun signature of CP violation (CPV) in neutrino oscillation experiments. In the intensity frontier, the currently running and upcoming high-precision long-baseline (LBL) neutrino oscillation experiments are the most promising avenues to unravel the novel signatures of CPV. One of the prime scientific goals of these LBL experiments is to provide an explicit demonstration of leptonic CPV by precisely measuring the differences between the θ_{13} -driven oscillations of muon-type neutrinos and antineutrinos into electron-type neutrinos and antineutrinos, respectively.

By observing these differences, the currently running LBL experiments T2K [8, 9] and NOvA [10] have already started probing the parameters space of δ_{CP} and provided crucial hints towards non-zero CPV. Now, it bestows upon the next-generation LBL experiments in the neutrino roadmap to convert these crucial hints of leptonic CPV into discoveries at high confidence level. Such a path-breaking discovery would certainly pave the way to elucidate the age-old flavor puzzle and the prevalence of matter over antimatter in the Universe [1, 11–14].

In this paper, after having an insightful discussion on the critical role of intrinsic, extrinsic, and total CP asymmetries in the appearance channel and extrinsic CP asymmetries in the disappearance channel, we study in detail the capabilities of the next-generation long-baseline neutrino oscillation experiments DUNE (Deep Underground Neutrino Experiment) [15–20] and T2HK¹ (Tokai to Hyper-Kamiokande) [21, 22] in isolation and combination to establish the leptonic CPV ($\delta_{\text{CP}} \neq 0^\circ$ and 180°) at 3σ confidence level for at least 75% choices² of true δ_{CP} in its entire range of -180° to 180° , considering the state-of-the-art simulation details of these facilities. We extend our analysis to the proposed T2HKK³ setup [23] and explore its CP coverage in standalone mode and also in combination with DUNE. The main thrust of this paper is to investigate in detail the possible complementarity among these high-precision experiments [24–29] to fully exploit the three-flavor interference effects [30] suppressing the parameter degeneracies, which in turn enhances the CP coverage. The key point of our analysis is to demonstrate how these experiments bring complementary information on the CP phase δ_{CP} for different octant choices of the 2-3 mixing angle (θ_{23}) at different L/E values, by means of appearance and disappearance channels in neutrino and antineutrino modes. Such a combination is also crucial to tackle the underlying degeneracies among θ_{23} and δ_{CP} , which reduce the CP coverage in δ_{CP} [31, 32] while establishing the leptonic CPV.

¹This experiment plans to house a 187 kt water Cherenkov far detector at a distance of 295 km from the J-PARC facility with an off-axis angle of 2.5° , which we often refer as Japanese detector (JD).

²We often mention this performance indicator of a given experiment as “CP coverage”, which denotes the values of true δ_{CP} (in %) in its entire range of $[-180^\circ, 180^\circ]$, for which leptonic CPV can be established at $\geq 3\sigma$ confidence level.

³This setup consists of two water Cherenkov far detectors (187 kt each): the first detector in Japan (JD) and the second detector in Korea (KD) at a distance of 295 km and 1100 km from the J-PARC facility, respectively. The JD (KD) will receive the same off-axis (2.5°), narrow-band beam from the J-PARC facility covering the first (second) oscillation maximum. We often denote this setup as JD+KD in this paper.

The upcoming DUNE is planning to use a 40 kt liquid argon time projection chamber (LArTPC) as a far detector which will be exposed to an on-axis, high-intensity, wide-band neutrino beam covering both the first and second oscillation maxima with a baseline of 1300 km. The DUNE far detector is expected to have an unmatched kinematic reconstruction capability for all the observed particles in the final state, which plays an important role to reject a large fraction of the neutral current background. The presence of an efficient near detector will significantly minimize the impact of flux and cross-section related systematic uncertainties at the DUNE far detector. DUNE will experience a significant amount of Earth's matter effect because of its relatively large baseline of 1300 km and having an access to a wide-band beam whose flux extends up to ~ 6 GeV with a peak at around 2.5 GeV. All these features help DUNE to settle the issue of neutrino mass ordering⁴ at a very high confidence level irrespective of the choices of other oscillation parameters and to measure the values of δ_{CP} and θ_{23} with satisfactory precision utilizing the information on oscillation pattern at several L/E values [17, 18]. On the other hand, in Japan, the proposed gigantic 187 kt Hyper-Kamiokande (HK) water Cherenkov detector will serve as the far detector for the T2HK (JD) setup at a distance of 295 km from the J-PARC facility and receive an off-axis (2.5°), upgraded, narrow-band beam with a flux peaking around the first oscillation maximum of ~ 0.6 GeV. The relatively shorter baseline and high statistics help T2HK (JD) to achieve an unparalleled precision in the measurement of δ_{CP} and θ_{23} free from Earth's matter effect [21, 22]. The Korean detector (KD) with a baseline of 1100 km and an off-axis beam from J-PARC having a peak around the second oscillation maximum, is slightly sensitive to Earth's matter effect and provides complementary information on δ_{CP} as compared to JD [23].

In this paper, we study in detail how the coverage in δ_{CP} for $\geq 3\sigma$ leptonic CPV varies with the choice of θ_{23} , exposure, optimal runtime in neutrino and antineutrino modes, and systematic uncertainties in these experiments in isolation and combination. We find that neither DUNE nor T2HK individually can achieve the milestone of 75% CP coverage for which at least 3σ leptonic CPV can be ensured, with their nominal exposures and systematic uncertainties. In DUNE, we observe that the main bottleneck is $\theta_{23} - \delta_{\text{CP}}$ degeneracy which appears in the picture when θ_{23} lies in the range of 42° to 48° . We notice that this degeneracy cannot be resolved in DUNE even by doubling the exposure or reducing the current systematic uncertainties by a factor of two. While in T2HK, although such degeneracy does not play any significant role because of the negligible matter effects, the current systematic uncertainties are an obstacle in achieving the above-mentioned sensitivity. One of the important conclusions of our work is that the complementarity between DUNE and T2HK is essential to obtain the desired CP coverage irrespective of the value of θ_{23} in Nature. Our study shows that for the combination of DUNE and T2HK, only half of their nominal exposures are sufficient to establish 3σ leptonic CPV for at least 75% choices of δ_{CP} for almost all values of θ_{23} , with their nominal systematic uncertainties. This becomes possible due to the less systematic uncertainties in DUNE as compared to T2HK and high

⁴The sign of Δm_{31}^2 ($\equiv m_3^2 - m_1^2$) is still unknown. If $\Delta m_{31}^2 > 0$, it is known as normal mass ordering (NMO) ($m_3 \gg m_2 > m_1$), while if $\Delta m_{31}^2 < 0$, it is referred to as inverted mass ordering (IMO) ($m_2 > m_1 \gg m_3$).

matter-independent disappearance statistics in T2HK, that helps in constraining θ_{23} in a narrow range and thus to resolve the $\theta_{23} - \delta_{\text{CP}}$ degeneracy. We find that with an improved systematic uncertainty of 2.7% in appearance mode, the standalone T2HK (JD) setup can provide a CP coverage of around 75% for almost all values of θ_{23} with nominal exposure. We observe that with nominal exposure and systematic uncertainties, T2HKK (JD+KD) can also achieve the 75% CP coverage for all values of θ_{23} , but its CP coverage is always less than that of DUNE+JD. At the same time, with only half of their exposures and nominal systematic uncertainties, T2HKK+DUNE can achieve a CP coverage of more than 80% for almost all values of θ_{23} .

We organize the paper as follows. We initiate our discussion with a detailed analytical understanding of CP asymmetry in Sec. 2, which will come in handy while analyzing our findings. In Sec. 3, we outline our experimental and simulation details of different setups under consideration. Sec. 4 culminates our results and findings wherein we discuss our milestone of achieving 3σ leptonic CPV for at least 75% choices of δ_{CP} in these experiments in isolation and combination as a function of (a) true $\sin^2 \theta_{23}$ in Sec. 4.1, (b) varying exposure in Sec. 4.2, (c) optimal runtime in neutrino and antineutrino modes in Sec. 4.3, and (d) systematic uncertainties in Sec. 4.4. Also, in Sec. 4.5, we estimate the enhanced CP coverage of these experiments when we assume the values of true δ_{CP} only in its current 3σ allowed range of $[-175^\circ, 41^\circ]$, instead of its entire range of $[-180^\circ, 180^\circ]$. Finally, we summarize with our concluding remarks in Sec. 5.

2 Discussion at the Oscillation Probability Level

The mixing matrix in the standard three-neutrino (3ν) framework is written in terms of the three mixing angles (θ_{23} , θ_{13} , and θ_{12}) and one complex phase (δ_{CP}) [33]. Following the usual PMNS parameterization, we have :

$$U_{\text{PMNS}} = \begin{pmatrix} c_{12}c_{13} & s_{12}c_{13} & s_{13}e^{-i\delta_{\text{CP}}} \\ -s_{12}c_{23} - c_{12}s_{23}s_{13}e^{i\delta_{\text{CP}}} & c_{12}c_{23} - s_{12}s_{23}s_{13}e^{i\delta_{\text{CP}}} & s_{23}c_{13} \\ s_{12}s_{23} - c_{12}c_{23}s_{13}e^{i\delta_{\text{CP}}} & -c_{12}s_{23} - s_{12}c_{23}s_{13}e^{i\delta_{\text{CP}}} & c_{23}c_{13} \end{pmatrix},$$

where we notice that the Dirac phase δ_{CP} is always coupled to the mixing angles. This explains that sensitivity in the CP phase strongly depends on the knowledge of other mixing parameters. At LBL experiments, we mostly probe the $\nu_\mu(\bar{\nu}_\mu) \rightarrow \nu_\mu(\bar{\nu}_\mu)$ (disappearance) and the $\nu_\mu(\bar{\nu}_\mu) \rightarrow \nu_e(\bar{\nu}_e)$ (appearance) channels. Following the approach in Ref. [34], we can further simplify the appearance probability expression in Ref. [35] that considers series expansion up to the second order term in α and $\sin \theta_{13}$ as follows

$$P_{\mu e} \approx N \sin^2 \theta_{23} + O \sin 2\theta_{23} \cos(\Delta + \delta_{\text{CP}}), \quad (2.1)$$

where,

$$N = 4 \sin^2 \theta_{13} \frac{\sin^2[(\hat{A} - 1)\Delta]}{(\hat{A} - 1)^2}, \quad (2.2)$$

$$O = 2\alpha \sin \theta_{13} \sin 2\theta_{12} \frac{\sin \hat{A} \Delta \sin[(\hat{A} - 1)\Delta]}{\hat{A}(\hat{A} - 1)}. \quad (2.3)$$

This grouping of terms helps to visualize the dependence on the atmospheric mixing angle (θ_{23}). In the above set of equations, $\Delta = \Delta m_{31}^2 L/4E$, $\alpha = \Delta m_{21}^2/\Delta m_{31}^2$, and $\hat{A} = A/\Delta m_{31}^2$, wherein the Wolfenstein matter term, $A = 2\sqrt{2}G_F N_e E \approx 7.6 \times Y_e \times 10^{-14} \times \rho_{\text{avg}}$ (g/cm^3) $\times E$ (GeV). Here ρ_{avg} is the line-averaged constant Earth matter density which we consider as $2.848 \text{ g}/\text{cm}^3$, $2.7 \text{ g}/\text{cm}^3$, and $2.8 \text{ g}/\text{cm}^3$ in DUNE [36], JD [22], and KD [23], respectively. Also, assuming that Earth's matter is electrically neutral and isoscalar, we obtain $N_e = N_p = N_n$ where N_p and N_n are proton and neutron number densities in Earth, respectively. Thus, the relative number density given by: $Y_e \equiv N_e/(N_p + N_n)$ is estimated as 0.5. Further, from Eq. 2.1, we observe that the CP-violating term contains $\sin 2\theta_{23}$ and thus is insensitive to the octant of the atmospheric angle [37–42]. Moreover, changing from neutrino to antineutrino mode notably changes signs of \hat{A} , thus leading to matter-induced or fake (extrinsic) CPV [43–45]. This will have a dominant contribution as it is present in the coefficient of the leading term: N (refer to Eq. 2.2). While the presence of the Dirac CP phase in the sub-leading term gives rise to the genuine (intrinsic) CPV (refer to Eq. 2.3).

$\sin^2 \theta_{12}$	$\sin^2 \theta_{23}$	$\sin^2 \theta_{13}$	Δm_{31}^2 (eV ²) $\times 10^{-3}$	Δm_{21}^2 (eV ²) $\times 10^{-5}$	δ_{CP} ($^\circ$)	Mass Ordering
0.303	[0.4 , 0.6]	0.0223	2.522	7.36	[- 180 , 180]	NMO

Table 1: The benchmark values of six oscillation parameters used in our analysis assuming normal mass ordering (NMO).

To probe CPV in oscillation experiments, one needs to note the difference between neutrino and antineutrino oscillation probabilities. The quantity which is strongly correlated to the sensitivity in δ_{CP} is the CP asymmetry [46–49]. In the following subsections, we will discuss how CP asymmetries affect CPV at the probability level. Throughout our simulation, we use the constant values of θ_{12} , θ_{13} , Δm_{21}^2 , and Δm_{31}^2 as our benchmark values (refer to Table 1). We often vary θ_{23} in some cases as will be mentioned wherever necessary, while δ_{CP} is always varied in its entire range, except for Sec 4.5 where we make use of the current 3σ constraints.

2.1 Extrinsic, Intrinsic, and Total CP Asymmetries in Appearance Channel

The CP asymmetry in the appearance channel is defined as

$$\mathcal{A}_{\text{CP}}^{\mu e} = \frac{P_{\mu e} - \bar{P}_{\mu e}}{P_{\mu e} + \bar{P}_{\mu e}}. \quad (2.4)$$

Different expansions have been done to understand the behavior of such asymmetry in terms of mixing angles [50]. However, to realize the role of the atmospheric mixing angle in the δ_{CP} sensitivity, we fix remaining mixing angles at their benchmark values ($\sin \theta_{13} \sim 1/7$ and $\sin \theta_{12} \sim 1/\sqrt{3}$). Also, since the value of matter parameter in the considered LBL

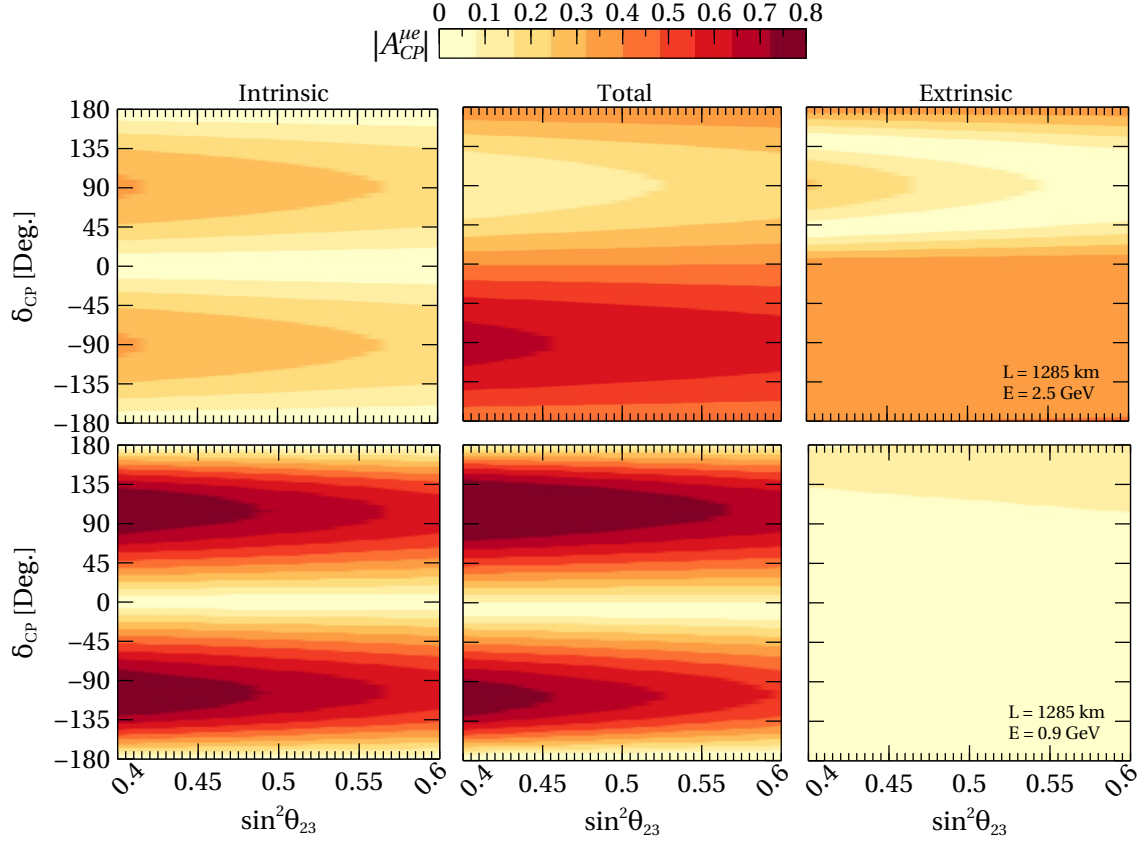


Figure 1: Absolute CP asymmetry ($|\mathcal{A}_{CP}^{\mu e}|$) as a function of δ_{CP} and $\sin^2 \theta_{23}$ for first oscillation maximum ($L = 1285$ km, $E = 2.5$ GeV) and second oscillation maximum ($L = 1285$ km, $E = 0.9$ GeV) in DUNE, assuming NMO are shown in the top and bottom panels, respectively. The left and middle panels in both top and bottom are obtained in a vacuum (intrinsic or genuine $\mathcal{A}_{CP}^{\mu e}$) and finite matter density (both intrinsic and extrinsic $\mathcal{A}_{CP}^{\mu e}$) scenarios, respectively. While the right panel represents the difference between the first two (only extrinsic or fake $\mathcal{A}_{CP}^{\mu e}$). Values of other oscillation parameters are taken from Table 1.

experiments is not large, we can expand in \hat{A} up to the first order. The resulting asymmetry is written as follows:

$$\mathcal{A}_{CP}^{\mu e} = [\mathcal{A}_{CP}^{\mu e}]_{\text{vac}} + \hat{A}[\mathcal{A}_{CP}^{\mu e}]_{\text{mat}} + \mathcal{O}(\hat{A}^2), \quad (2.5)$$

where

$$[\mathcal{A}_{CP}^{\mu e}]_{\text{vac}} = \frac{-28\alpha\Delta \cos \theta_{23} \sin \delta_{CP} \sin \Delta}{3\sqrt{2} \sin \theta_{23} \sin \Delta + 28\alpha\Delta \cos \theta_{23} \cos \delta_{CP} \cos \Delta} \quad (2.6)$$

$$[\mathcal{A}_{CP}^{\mu e}]_{\text{mat}} = -\sin^2 \theta_{23} (\Delta \cos \Delta - \sin \Delta) \frac{126\alpha\Delta \cos \theta_{23} \cos \delta_{CP} \cos \Delta + 18 \sin^2 \theta_{23} \sin \Delta}{(3 \sin^2 \theta_{23} \sin \Delta + 7\sqrt{2}\alpha \cos \delta_{CP} \cos \Delta \sin^2(2\theta_{23}))^2} \quad (2.7)$$

It is clear that, when the value of θ_{23} increases, the denominator of both the contributing term in Eq. 2.6 and Eq. 2.7 increases. For this reason, the absolute value of the asymmetry

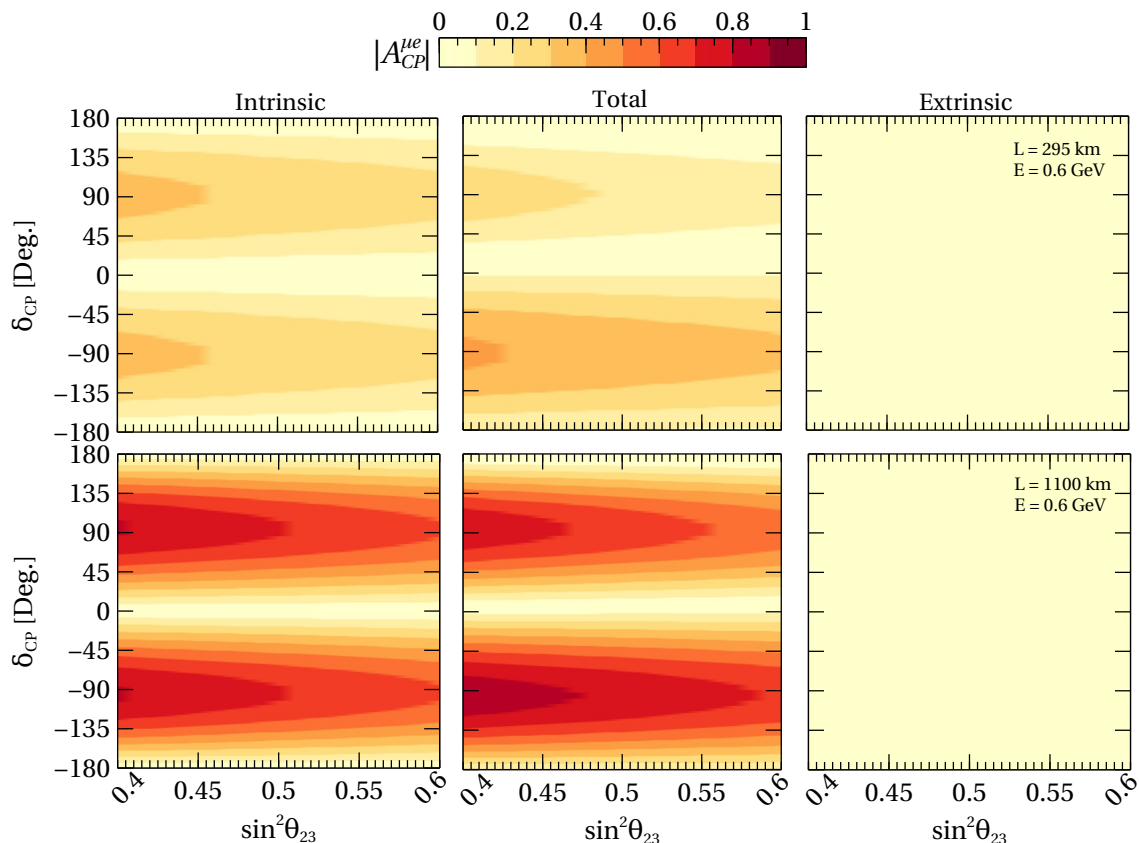


Figure 2: $|A_{CP}^{\mu e}|$ as a function of δ_{CP} and $\sin^2 \theta_{23}$ for first oscillation maximum in JD ($L = 295$ km, $E = 0.6$ GeV) and second oscillation maximum in KD ($L = 1100$ km, $E = 0.6$ GeV) assuming NMO are shown in the top and bottom panels, respectively. The left and middle panels in both top and bottom are obtained in vacuum (intrinsic or genuine $A_{CP}^{\mu e}$) and finite matter density (intrinsic $A_{CP}^{\mu e}$ + extrinsic $A_{CP}^{\mu e}$) scenarios, respectively. While the right panel represents the difference between the first two (only extrinsic or fake $A_{CP}^{\mu e}$). Values of other oscillation parameters are taken from Table 1.

becomes smaller, and we expect less CPV sensitivity. So, at the first oscillation maximum, ($\Delta = \pi/2$)⁵ the asymmetry reduces to:

$$A_{CP}^{\mu e} \approx -\frac{7}{3}\alpha\sqrt{2}\pi \cot \theta_{23} \sin \delta_{CP} + 2\hat{A}, \quad (2.8)$$

whose modulus decreases with an increase in θ_{23} . The genuine or intrinsic CP has a sign opposite to the extrinsic or fake matter-induced contribution. Thus, there exists some combination of θ_{23} and $\delta_{CP} \in [0^\circ, 180^\circ]$, such that this asymmetry vanishes. It is interesting to note that the vacuum contribution becomes three times larger when considering the second oscillation maximum ($\Delta = 3\pi/2$). Therefore, observing the CPV at such L/E

⁵To be maximally sensitive to the oscillation probability, we must have $\Delta = (2n + 1)\frac{\pi}{2}$, where $n = 0, 1, 2, \dots$

combination can give much more sensitivity to the δ_{CP} [51–53]. The exact numerical behavior of the CP asymmetry in the appearance channel ($|\mathcal{A}_{\text{CP}}^{\mu e}|$) is shown in Fig. 1 for ($L = 1285$ km, $E = 2.5$ GeV), ($L = 1285$ km, $E = 0.9$ GeV) which corresponds to the first and second oscillation maxima in DUNE. For each L/E combination, we show three panels: in the left column, we show the vacuum or δ_{CP} -induced contribution (intrinsic). In the center, we illustrate the total asymmetry, and in the right column, we display the contribution due to the matter effects (extrinsic). In all the panels, we only plot the absolute value of the asymmetries since, in this work the most important aspect is to stress on the difference between the asymmetries in the CP-violating and the CP-conserving cases. From the top left panel in Fig. 1, we observe that the intrinsic contribution is the same in both the maximal CP-violating values of δ_{CP} (90 and -90°). Moreover, keeping the CP phase fixed to any value, the asymmetry reduces when we increase the value of θ_{23} from lower octant⁶ (LO) to higher octant (HO) (as expected from Eq. 2.6 and Eq. 2.7). Contrastingly, the extrinsic CP asymmetry (top right panel), which occurs solely due to the matter effect, is asymmetric, being larger for favorable δ_{CP} in NMO (negative half plane) and smaller for unfavorable δ_{CP} in NMO (positive half plane). Therefore, the total asymmetry (middle panel) is no longer the same for the maximal CP-violating values of δ_{CP} . Further, due to contribution from \hat{A} , the intrinsic $|\mathcal{A}_{\text{CP}}^{\mu e}|$, which is zero at CP-conserving values ($\delta_{\text{CP}} = 0^\circ$ and 180°), now has a finite value. Hence, from the top middle panel, it is clear that the asymmetries in CP-violating cases tend to shift closer to the CP-conserving value when θ_{23} increases. For the bottom row, where we plot the CP asymmetry at the second oscillation maxima ($E = 0.9$ GeV), the matter effect becomes less, and the intrinsic component completely dominates the total asymmetry. Moreover, the asymmetry values are amplified in the bottom panel, which we expect as here the L and E are similar to the second oscillation maximum in DUNE. Similarly, in Fig. 2, we plot the CP asymmetry for the T2HK (JD) setup with $L = 295$ km and $E = 0.6$ GeV at the first oscillation maxima (top row) and T2HKK with $L = 1100$ km and $E = 0.6$ GeV at the second oscillation maxima (bottom row). The top panel does not observe any significant contribution in the extrinsic panel, due to less matter effect ($L = 295$ km). Thus, we expect the J-PARC based experiments to provide a cleaner environment for the measurements in δ_{CP} , even though the values reached by the asymmetries in these cases are not as high as the DUNE. On the other hand, the bottom panels of Fig. 2, which correspond to the second oscillation maximum L/E choice for T2HKK, behave just like the bottom panels in Fig. 1.

2.2 Extrinsic CP Asymmetry in Disappearance Channel

The ν_μ disappearance channel, being T invariant, is directly CP-conserving in a vacuum-like scenario. However, the Earth matter potential interacts differently with neutrinos and antineutrinos, which can further induce a fake or extrinsic CPV in this channel [48, 50]. Thus, although the disappearance channel does not directly affect the measurements in CP phase, it is important to realize its ability to generate fake or extrinsic CPV. This is

⁶Existence of non-maximal θ_{23} gives rise to two degenerate solutions: $\theta_{23} < 45^\circ$ (LO) and $\theta_{23} > 45^\circ$ (HO).

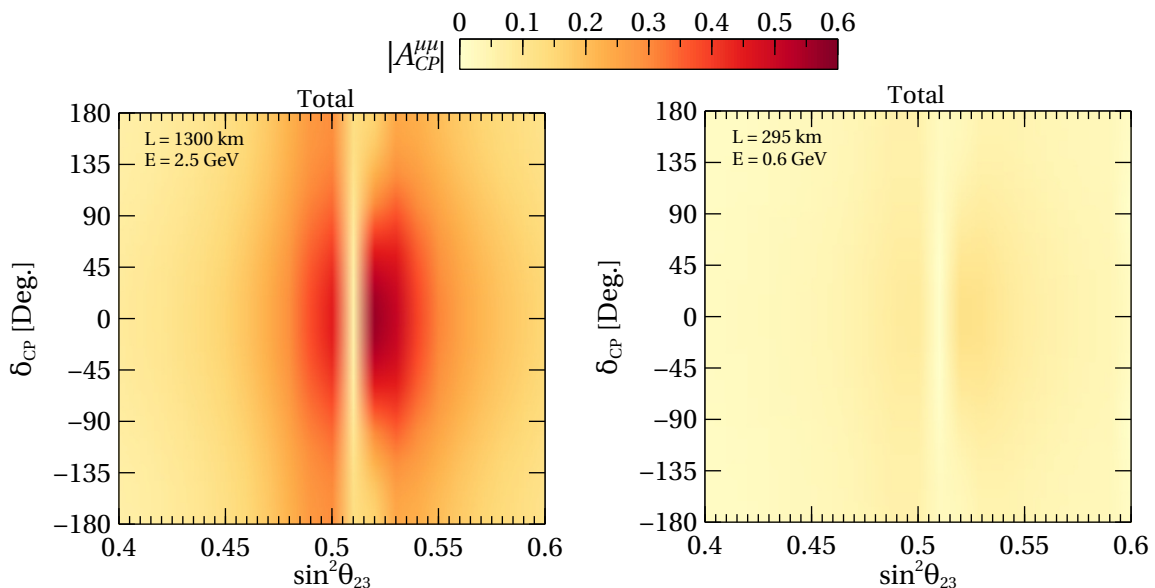


Figure 3: $|A_{\text{CP}}^{\mu\mu}|$ as a function of δ_{CP} and $\sin^2 \theta_{23}$ assuming NMO for first oscillation maximum in DUNE ($L = 1285$ km, $E = 2.5$ GeV) and JD ($L = 295$ km, $E = 0.6$ GeV) is shown in the left and right panel, respectively. Values of other oscillation parameters are taken from Table 1.

crucial in our study as we will discuss later its effect in our results (Sec. 4.1). Following the same convention, as discussed in Ref. [34], we write the disappearance probability as

$$P_{\mu\mu} \approx 1 - M \sin^2(2\theta_{23}) - N \sin^2 \theta_{23} - R \sin 2\theta_{23} + T \sin 4\theta_{23}, \quad (2.9)$$

where:

$$M = \sin^2 \Delta - \alpha \cos^2 \theta_{12} \Delta \sin 2\Delta + \frac{2}{\hat{A} - 1} \sin^2 \theta_{13} \left(\sin \Delta \cos(\hat{A}\Delta) \frac{\sin[(\hat{A} - 1)\Delta]}{\hat{A} - 1} - \frac{\hat{A}}{2} \Delta \sin 2\Delta \right), \quad (2.10)$$

$$R = 2\alpha \sin \theta_{13} \sin 2\theta_{12} \cos \delta_{\text{CP}} \cos \Delta \frac{\sin \hat{A}\Delta \sin[(\hat{A} - 1)\Delta]}{\hat{A}(\hat{A} - 1)}, \quad (2.11)$$

$$T = \frac{1}{\hat{A} - 1} \alpha \sin \theta_{13} \sin 2\theta_{12} \cos \delta_{\text{CP}} \sin \Delta \left(\hat{A} \sin \Delta - \frac{\sin \hat{A}\Delta}{\hat{A}} \cos[(\hat{A} - 1)\Delta] \right). \quad (2.12)$$

and N has already been defined in Eq. 2.2. The detailed analytical discussion of fake CP asymmetry in the disappearance channel results in a cumbersome expression. However, for first oscillation minima ($\Delta = \pi/2$) and the approximated numerical values of the solar and the reactor mixing angles ($\sin \theta_{12} = 1/\sqrt{3}$ and $\sin \theta_{13} = 1/7$), one can calculate the CP asymmetry in the $\nu_\mu \rightarrow \nu_\mu$ disappearance channel which is defined as

$$\mathcal{A}_{\text{CP}}^{\mu\mu} = \frac{P_{\mu\mu} - \bar{P}_{\mu\mu}}{P_{\mu\mu} + \bar{P}_{\mu\mu}} \quad (2.13)$$

Substituting the discussed approximation in above expression and neglecting the higher order terms, we get

$$\mathcal{A}_{\text{CP}}^{\mu\mu} \approx \hat{A} \frac{24 \sin^2 \theta_{23} + 7\sqrt{2}(\pi^2 - 4)\alpha \cos \delta_{\text{CP}} \sin 2\theta_{23}}{6 + 141 \cos 2\theta_{23}}. \quad (2.14)$$

This asymmetry increases with the increase in θ_{23} until the expansion breaks at $\cos 2\theta_{23} = -6/141$. This occurs for $\sin^2 \theta_{23} > 0.5$ (HO). While after this value, the magnitude of asymmetry starts decreasing with the increase in θ_{23} . In Fig. 3, we exhibit the absolute value of the disappearance asymmetry ($|\mathcal{A}_{\text{CP}}^{\mu\mu}|$) for ($L = 1285$ km, $E = 2.5$ GeV) and ($L = 295$ km, $E = 0.6$ GeV) that also corresponds to DUNE and JD at their respective first oscillation maxima energy. We do not show the plots corresponding to the second oscillation maxima since the fake CP asymmetry in disappearance is solely due to the interaction with the Earth matter potential, whose effect becomes minimal in such conditions. Thus, we do not expect $\mathcal{A}_{\text{CP}}^{\mu\mu}$ in DUNE and KD working at their second oscillation maxima to have any significant contribution to our analysis. We notice that JD, bearing a relatively smaller baseline ($L = 295$ km) has very small matter effects and thus exhibit very minute fake asymmetry even at first oscillation maximum, as shown in the right panel of Fig. 3. On the other hand, DUNE has a larger baseline ($L = 1285$ km), thus exhibiting consequential $|\mathcal{A}_{\text{CP}}^{\mu\mu}|$ that reaches as high as ≈ 0.6 (see the left panel in Fig. 3), which is almost comparable to the total $|\mathcal{A}_{\text{CP}}^{\mu e}|$ (≈ 0.8) (see the top middle panel in Fig. 1). We observe that $|\mathcal{A}_{\text{CP}}^{\mu\mu}|$ is minimal at the two extremes of octant of θ_{23} for any value of δ_{CP} . The asymmetry gradually increases while proceeding towards the maximal mixing (MM) corresponding to $\sin^2 \theta_{23} = 0.5$, from either side for almost all δ_{CP} . However, $|\mathcal{A}_{\text{CP}}^{\mu\mu}|$ manifests two maxima around $\delta_{\text{CP}} = 0^\circ$, one each in the two octants: LO ($\sin^2 \theta_{23} \approx 0.49$) and HO ($\sin^2 \theta_{23} \approx 0.52$). As discussed previously in the analysis of Eq. 2.14, we observe a critical point in HO in the figure as well, around which the nature of $\mathcal{A}_{\text{CP}}^{\mu\mu}$ changes. Correspondingly, around this point our analytical expansion also breaks. However, in our expression this completely vanishes ($\mathcal{A}_{\text{CP}}^{\mu\mu} \approx 0$) as we have neglected the higher order terms. This nature of fake $\mathcal{A}_{\text{CP}}^{\mu\mu}$ is crucial in our result, as we will elaborate on this further in our results (Sec. 4.1).

2.3 $\theta_{23} - \delta_{\text{CP}}$ Degeneracy

From the above discussion, we observe that the value of the atmospheric mixing angle can influence CPV sensitivity. We can further expect this sensitivity to be affected by the octant of $\theta_{23} - \delta_{\text{CP}}$ degeneracy in appearance channel [54–56]. The persisting issue of octant of θ_{23} [37] makes it highly probable for some $\bar{\theta}_{23}$ and $\bar{\delta}_{\text{CP}}$ to exist such that for a given θ_{23} , δ_{CP} ,

$$P_{\mu e}(\theta_{23}, \delta_{\text{CP}}) = P_{\mu e}(\bar{\theta}_{23}, \bar{\delta}_{\text{CP}}), \quad (2.15)$$

$$\bar{P}_{\mu e}(\theta_{23}, \delta_{\text{CP}}) = \bar{P}_{\mu e}(\bar{\theta}_{23}, \bar{\delta}_{\text{CP}}), \quad (2.16)$$

holds true. For instance, fixing $\theta_{23} = 45^\circ$, $\sin \theta_{13} = 1/7$, and $\sin \theta_{12} = 1/\sqrt{3}$ in presence of matter effect, $\nu_\mu \rightarrow \nu_e$ oscillation probability is given as:

$$P_{\mu e}(45^\circ, \delta_{\text{CP}}) = \frac{2 \sin[(A-1)\Delta]^2}{49(A-1)^2} + \frac{4\sqrt{2}\alpha \cos(\delta_{\text{CP}} + \Delta) \sin[(A-1)\Delta] \sin(A\Delta)}{21A(A-1)}. \quad (2.17)$$

Assuming that the degenerate atmospheric angle is not too far from the maximal value, we define it as $\bar{\theta}_{23} = 45^\circ + x$. Now, considering terms only up to the first order in x we obtain:

$$P_{\mu e}(45^\circ + x, \bar{\delta}_{\text{CP}}) = P_{\mu e}(45^\circ, \bar{\delta}_{\text{CP}}) + \frac{4x \sin[(A-1)\Delta]^2}{49(A-1)^2}. \quad (2.18)$$

For the above scenario, the system of equations in Eq. 2.15 and Eq. 2.16 reduces to the following two equations-

$$\frac{\sqrt{2}\alpha \sin(A\Delta)}{3A} [\cos(\Delta - \delta_{\text{CP}}) - \cos(\Delta - \bar{\delta}_{\text{CP}})] = x \frac{\sin[(A-1)\Delta]}{7(A-1)} \text{ and} \quad (2.19a)$$

$$\frac{\cos(\Delta + \delta_{\text{CP}}) - \cos(\Delta + \bar{\delta}_{\text{CP}})}{\cos(\Delta - \delta_{\text{CP}}) - \cos(\Delta - \bar{\delta}_{\text{CP}})} = \frac{\sin[(A-1)\Delta] (1+A)}{\sin[(A+1)\Delta] (A-1)}. \quad (2.19b)$$

So, for each value of Δ , the above two equations will have different solutions. Thus, in principle, spectral analysis can reduce the above-mentioned degeneracy. Then, it is clear that in the vacuum-like scenario ($A \rightarrow 0$), Eq. 2.19a gives $x = 0$, while in Eq. 2.19b $\bar{\delta}_{\text{CP}} = \delta_{\text{CP}}$. Therefore in an experiment with negligible matter effect, the role of this degeneracy will not be crucial in determining the sensitivity of δ_{CP} . While in the presence of substantial matter effect and taking as an example $\delta_{\text{CP}} = 90^\circ$, the above equations will always have a solution for $\bar{\delta}_{\text{CP}}$ except when $\Delta = \pi/2$. Moreover, we have checked that given a certain matter potential, there is always a value of $\Delta < \pi/2$, for which we obtain $\bar{\delta}_{\text{CP}} = 0$. This infers that, in the presence of matter effect, we can always have identical solutions for maximal CP-violating and a CP-conserving case. The corresponding value of x in such cases is always positive, implying that the degenerate solution lies in the higher octant. While on the other hand, when $\delta_{\text{CP}} = -90^\circ$, we obtain degenerate solutions for $\bar{\delta}_{\text{CP}}$, but to get the CP-conserving degenerate solution, we need to find a specific L/E ratio that exceeds the value which we obtain at the atmospheric peak. Moreover, in this case, the corresponding deviation of the mixing angle is negative; hence the degenerate solution lies in the lower octant.

Next, we discuss the $\theta_{23} - \delta_{\text{CP}}$ degeneracy when considering both disappearance and appearance channels. For the degeneracy to occur with all other mixing angles and mass-splittings kept fixed, there should exist $\bar{\theta}_{23}$ and $\bar{\delta}_{\text{CP}}$ such that

$$P_{\mu\mu}(\theta_{23}, \delta_{\text{CP}}) = P_{\mu\mu}(\bar{\theta}_{23}, \bar{\delta}_{\text{CP}}) \quad (2.20)$$

$$\bar{P}_{\mu\mu}(\theta_{23}, \delta_{\text{CP}}) = \bar{P}_{\mu\mu}(\bar{\theta}_{23}, \bar{\delta}_{\text{CP}}). \quad (2.21)$$

However, the disappearance probability only has a mild dependence on δ_{CP} , which plays an important role when there is a substantial matter effect and θ_{23} around maximal mixing, as elaborated previously in the discussion of Fig. 3. Otherwise, the disappearance channel precisely measures the atmospheric mixing angle in δ_{CP} independent way. Thus disappearance channel helps in constraining θ_{23} when it is not around maximal mixing, which reduces the effect of $\theta_{23} - \delta_{\text{CP}}$ degeneracy for these θ_{23} in the appearance channel as well. Thus a combined analysis between the appearance and disappearance channels

is expected to break the $\theta_{23} - \delta_{\text{CP}}$ degeneracy only if (a) the matter effects are negligible or (b) true values of the atmospheric mixing angle are far away from the maximal mixing scenario, which for DUNE is true if $\sin^2 \theta_{23} \notin [0.48, 0.55]$ (refer to the discussion around Fig. 3). Therefore, in this region we obtain a θ_{23} independent δ_{CP} measurement.

3 Experimental Features and Simulation Details

Characteristics	DUNE	JD/KD
Baseline (km)	1285	295 (1100)
ρ_{avg} (g/cm ³)	2.848	2.7 (2.8)
Beam	LBNF [16]	J-PARC [57]
Beam Type	wide-band, on-axis	narrow-band, 2.5° off-axis
Beam Power	1.2 MW	1.3 MW
Proton Energy	120 GeV	30 GeV
P.O.T./year	1.1×10^{21}	2.7×10^{22}
Flux peaks at (GeV)	2.5	0.6
1 st (2 nd) oscillation maxima for appearance channel (GeV)	2.6 (0.87)	0.6 (0.2) / 1.8 (0.6)
Detector mass (kt)	40, LArTPC	187 each, water Cherenkov
Runtime ($\nu + \bar{\nu}$) yrs	5 + 5	2.5 + 7.5
Exposure (kt·MW·yrs)	480	2431
Signal Norm. Error (App.)	2%	5%
Signal Norm. Error (Disapp.)	5%	3.5%
Binned-events matched with	[19]	[23]

Table 2: Essential experimental features of various long-baseline experiments considered in our analysis. The first column characterizes DUNE while the second column depicts aspects of JD and KD.

The LBL accelerator experiments allow us to probe neutrino oscillation phenomena in a very controlled environment with fixed baselines and well-known energy spectra of neutrinos [58–61]. Over the last two decades or so, various LBL experiments have contributed significantly in measuring the three-flavor oscillation parameters with high precision [2, 7]. These experiments have access to both $\nu_{\mu} \rightarrow \nu_e$ appearance and $\nu_{\mu} \rightarrow \nu_{\mu}$ disappearance channels⁷ with a very well-determined initial *muon* neutrino flux. The upcoming next-generation LBL experiments are expected to resolve all the degeneracies [38, 66–68] among the three-flavor neutrino oscillation parameters with a very high confidence level and improve the existing precision manifold.

⁷ ν_{τ} appearance channel can also be accessible in long-baseline experiments if neutrino energy is above the charged-current (CC) production threshold of τ lepton (≈ 3.1 GeV) [32, 62–65].

Parameter Experiment	θ_{23}	$\delta_{\text{CP}} = 0^\circ$ ($\nu_e, \bar{\nu}_e, \mathcal{N}_{\text{CP}}^{\mu e}$)	$\delta_{\text{CP}} = 90^\circ$ ($\nu_e, \bar{\nu}_e, \mathcal{N}_{\text{CP}}^{\mu e}$)	$\delta_{\text{CP}} = -90^\circ$ ($\nu_e, \bar{\nu}_e, \mathcal{N}_{\text{CP}}^{\mu e}$)
DUNE	40°	1965, 812, 0.41	1657, 857, 0.31	2303, 728, 0.52
	45°	2215, 875, 0.43	1902, 920, 0.34	2558, 790, 0.53
	50°	2470, 938, 0.45	2161, 982, 0.37	2807, 854, 0.53
JD	40°	1644, 1420, 0.074	1277, 1687, -0.14	2024, 1113, 0.29
	45°	1890, 1594, 0.085	1517, 1868, -0.1	2276, 1286, 0.28
	50°	2137, 1770, 0.093	1770, 2041, -0.07	2518, 1476, 0.26

Table 3: Total appearance event rates (signal + background) in neutrino, antineutrino modes, and $\mathcal{N}_{\text{CP}}^{\mu e}$ for DUNE (JD) corresponding to different sets of $\delta_{\text{CP}} : 0^\circ, 90^\circ, -90^\circ$ and $\theta_{23} : 40^\circ, 45^\circ, \text{ and } 50^\circ$ are shown in the second (third) set of rows, respectively.

In our analysis, we consider the two upcoming next-generation LBL experiments, DUNE and T2HK (JD). We also take into account the probable proposition of the second detector in Korea, the T2HKK (JD + KD) setup. The unprecedented high statistics, intense beam, and reduced systematic uncertainties in these experiments will be able to enhance precision measurements in oscillation parameters and possibly open the door for studying New Physics in the lepton sector. DUNE is proposed to bear a long baseline (1285 km) and so will be largely influenced by the matter effect, while JD, having relatively a much smaller baseline (295 km) will portray an almost vacuum-like scenario. Also, the flux in DUNE will peak at higher energies (~ 2.5 GeV), which enable the potential for searching for ν_τ appearance as well [63, 64, 69]. While the flux in JD will peak around ~ 0.6 GeV. Further, the DUNE far-detector will observe a wide-band on-axis beam, which allows for scanning several different L/E ratios (including the second oscillation maximum, which occurs at 0.9 GeV), while the JD detector will be receiving a narrow-band off-axis beam. In the JD + KD setup, the proposed second detector, KD in Korea (receiving the same flux as JD with a baseline of $L = 1100$ km), is expected to work at the second oscillation maximum. The DUNE will be a 40 kt LArTPC, with great imaging capabilities that will lower signal normalization uncertainties to just 2% in appearance and 5% in the disappearance. On the other hand, JD and KD, each will be 187 kt water Cherenkov detectors, which will accumulate huge statistics, however, with relatively poorer expected signal normalization uncertainties of 5% in the appearance channel and 3.5% in the disappearance. Further, the sources of backgrounds and their contribution in normalization uncertainties has been taken from Ref. [19, 23]. The proposed runtime ratio in JD/KD is in contrast with DUNE. While DUNE proposes a balanced run in neutrino and antineutrino mode, T2HK will be running in the ratio of 1:3 in $\nu : \bar{\nu}$ mode to ensure similar statistics from both the modes. In Table 2, we enlist characteristic attributes in these next-generation experiments that sum up their complementary features.

In Table 3, we summarize the number of neutrino and antineutrino events for DUNE and JD for three different choices of δ_{CP} ($0^\circ, 90^\circ, -90^\circ$) and three choices of θ_{23} : LO (40°), MM (45°), and in the HO (50°). For the sake of comparison, we also compute the values

of the integrated asymmetries, defined as

$$\mathcal{N}_{\text{CP}}^{\mu e} = \frac{N_{\mu e} - \bar{N}_{\mu e}}{N_{\mu e} + \bar{N}_{\mu e}}, \quad (3.1)$$

where $N_{\mu e}$ ($\bar{N}_{\mu e}$) is the number of events in the neutrino (antineutrino) mode. JD statistics is higher than the DUNE due to the higher exposure: 2431 kt·MW·yrs in the J-PARC based and 480 kt·MW·yrs in the Fermilab based experiment. Moreover, as expected, for the favorable choice of parameters, i.e., NMO, $\delta_{\text{CP}} = -90^\circ$ ($\delta_{\text{CP}} = 90^\circ$), and HO, we observe the highest neutrino (antineutrino) events. The integrated asymmetries follow the same nature as we observe at the probability level (refer to Fig. 1). Here also $\mathcal{N}_{\text{CP}}^{\mu e}$ in the CP-violating case tends to come closer to its value in the CP-conserving case as θ_{23} increases in both the experiments.

4 Our Results

In this section, we discuss the abilities of DUNE, T2HK (JD), and their combination in achieving the landmark of 75% CP coverage in true δ_{CP} for leptonic CPV at 3σ C.L. for all the values of $\sin^2 \theta_{23}$ in Nature. We also explore the capability of the T2HKK (JD + KD) setup. Further, we also inspect the effect of changing overall exposure in each setup while determining the CP coverage. Next, we survey the optimal runtime in neutrino and antineutrino modes to effectively increase CP coverage in different experimental setups. Finally, we address the importance of systematic uncertainties and how their variation can significantly affect our results.

In our analysis, we define the CP coverage as the percentage of true δ_{CP} for which an experiment establishes at least a 3σ CPV sensitivity. For this, we generate our prospective data assuming the entire range of true $\delta_{\text{CP}} \in [-180^\circ, 180^\circ]$, while in the fit, we marginalize over the test $\delta_{\text{CP}} = 0^\circ$ and 180° and choose the minimum. We use the Poissonian χ^2 [70] and estimate the median sensitivity [71] of a given LBL experiment in the frequentist approach [72]. To evaluate the sensitivity towards leptonic CPV, we use the following definition of $\Delta\chi^2$:

$$\Delta\chi^2 = \min_{(\delta_{\text{CP}}^{\text{test}}, \theta_{23}, \lambda_1, \lambda_2)} \left[\chi^2(\delta_{\text{CP}}^{\text{true}}) - \chi^2(\delta_{\text{CP}}^{\text{test}} = 0^\circ \text{ and } 180^\circ) \right]. \quad (4.1)$$

The fit is performed by marginalizing over θ_{23} in its current 3σ range of [0.4, 0.6] while keeping all other parameters fixed at the benchmark values as mentioned in Table 1. The symbols λ_1 and λ_2 refer to the systematic pulls [73–76] on signal and background, respectively. The present global neutrino oscillation data [4–7] measures atmospheric mass splitting with a very high precision of 1.1%, which will further improve to 0.5% with six years of data taking by JUNO [77]. Therefore, we do not marginalize over the present uncertainty in Δm_{31}^2 . Also, we do not marginalize over the wrong mass ordering in any of the results as there are hints towards NMO from the global oscillation data [4–7]. Moreover, the currently running LBL experiments: NO ν A and T2K, and the atmospheric experiments: Super-K [78] and DeepCore [79] will further strengthen the mass ordering measurements

in the near future. Also, by the time DUNE will accumulate data for CPV searches, it is expected to have already fixed the mass ordering [17]. For all the simulations, we use the GLoBES software [80, 81].

4.1 Impact of θ_{23} on CP coverage

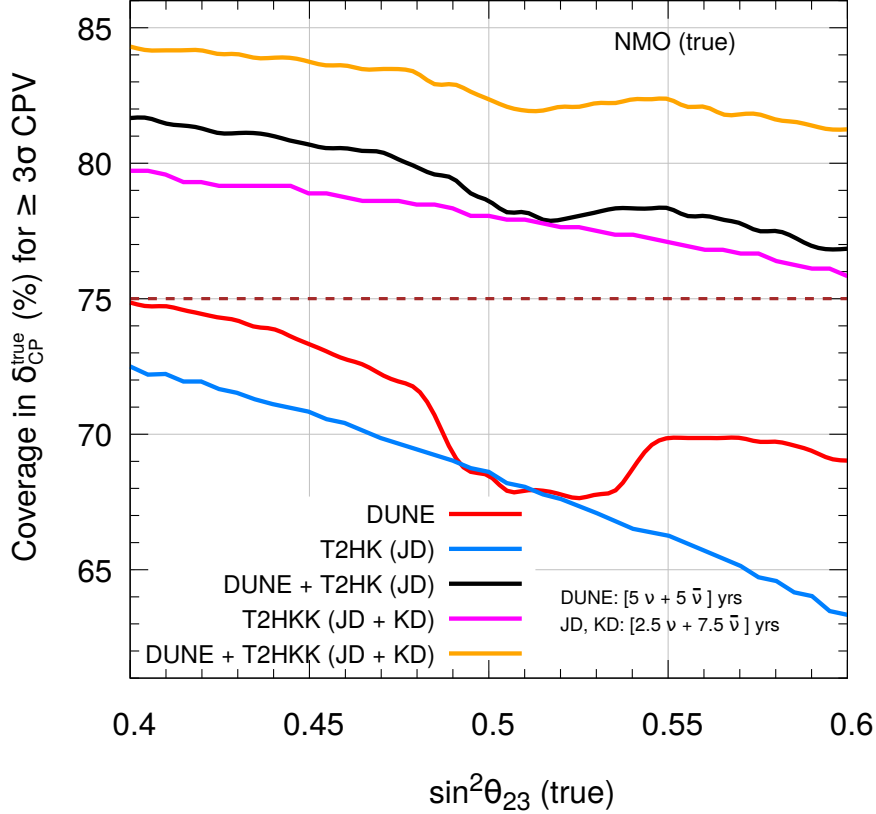


Figure 4: Coverage in true δ_{CP} for achieving $\geq 3\sigma$ leptonic CPV as a function of true $\sin^2 \theta_{23}$, when marginalized over the current 3σ uncertain range of $\sin^2 \theta_{23}$ $[0.4, 0.6]$ in the theory. The curves: red, blue, black, magenta, and orange are for DUNE, JD, DUNE + JD, JD + KD, and DUNE + JD + KD neutrino oscillation experiments, respectively. We assume true NMO, benchmark exposure, and the nominal runtime as mentioned in Table 2 in both data and theory.

As previously discussed in Sec. 2, the atmospheric mixing angle can play an important role in determining the CPV sensitivity. In Fig. 4, we depict how the ability of an experimental setup to measure CP coverage changes with the true value of $\sin^2 \theta_{23}$. We generate our data for each $\sin^2 \theta_{23}$ (true) by varying $\sin^2 \theta_{23}$ in our theory throughout the uncertain range of $[0.4, 0.6]$. Each colored curve corresponds to the CP coverage of a particular setup as a function of the true value of $\sin^2 \theta_{23}$. We observe that none of the individual experiments: DUNE (red curve) or JD (blue curve) can achieve the milestone of 75%. However, their combination makes CP coverage for the entire canvas of $\sin^2 \theta_{23}$

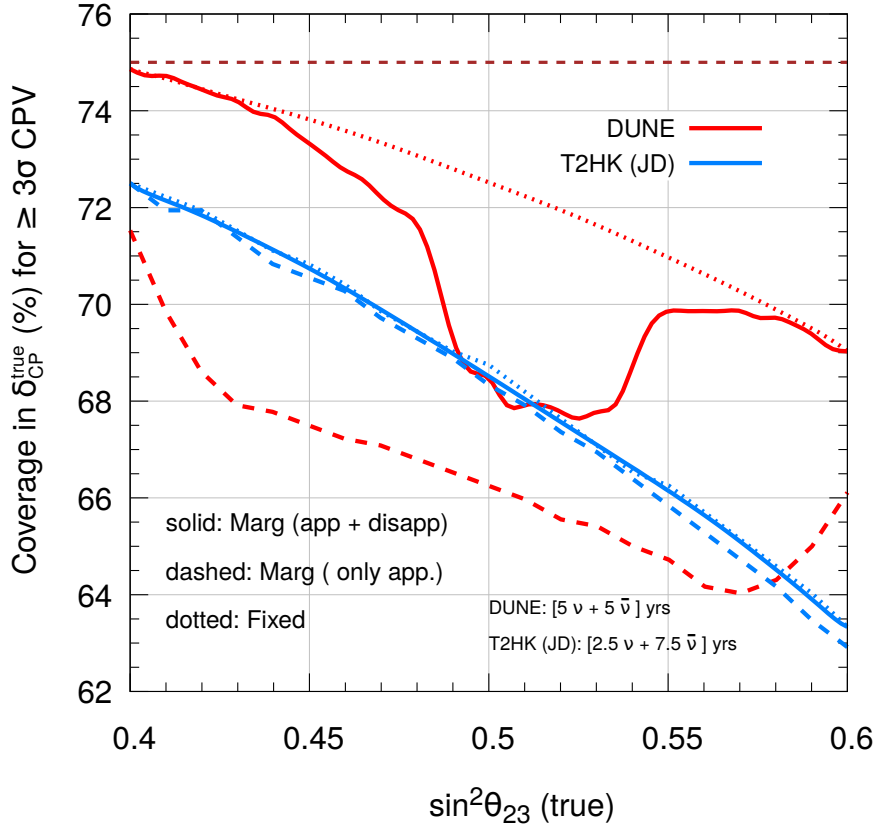


Figure 5: Coverage in true δ_{CP} for achieving $\geq 3\sigma$ leptonic CPV as a function of true $\sin^2 \theta_{23}$ assuming NMO. The solid curves are our result from Fig. 4, in which we generate data with both appearance and disappearance channels and marginalize over $\sin^2 \theta_{23}$ in its 3σ uncertain range of $[0.4, 0.6]$ in the fit. The dashed curves are obtained by generating our data with only appearance channel and marginalizing over $\sin^2 \theta_{23}$ in its 3σ uncertain range in the fit. While, the dotted curves correspond to our result by fixing identical $\sin^2 \theta_{23}$ in both data and fit (fixed-parameter scenario). The curves: red and blue correspond to DUNE and JD, respectively.

above 75%. This points out that the complementarity between DUNE and JD or JD and KD can help attain a better CP coverage irrespective of the $\sin^2 \theta_{23}$ value in Nature. Thus, if we are concerned about only CP coverage, there may be no remarkable advantages in adding a second detector to T2HK as DUNE + JD attains a better CP coverage than JD + KD combined. In all the setups, there is a general notion of CP coverage decreasing as we increase $\sin^2 \theta_{23}$ in the data; the reason for that can be found in the behavior of the appearance asymmetry, as previously discussed in text around figures 1 and 2. In DUNE, the 3σ CP coverage decreases from 75% to 68% when θ_{23} increases from 40° ($\sin^2 \theta_{23} = 0.4$) to 60° ($\sin^2 \theta_{23} = 0.6$), while in JD the coverage decreases from 73% to 63% of true δ_{CP} for the same. The performance of DUNE is observed to be better than JD, but not around

maximal mixing. DUNE and combined setups with DUNE (DUNE + JD and DUNE + JD + KD) exhibit an additional worsening around maximal mixing choices, which is absent in JD and JD + KD.

To further explore this, we try to understand this nature in individual setups: DUNE and JD. In Fig. 5, we represent CP coverage in three scenarios for both JD and DUNE. In the first (dotted blue and red curves) we fix the same value of atmospheric mixing angle in both theory and data; the second (solid blue and red curves) is the result from previously discussed Fig. 4, wherein we marginalize in theory over $\sin^2 \theta_{23}$ in the current 3σ uncertain range of $[0.4, 0.6]$; in the third (dashed blue and red curves) we show the contribution from only appearance channel marginalized over the allowed 3σ range in $\sin^2 \theta_{23}$. In the fixed parameter case, there is no role of $\theta_{23} - \delta_{\text{CP}}$ degeneracy since both are fixed to their true value in the fit. Thus, we see monotonically decreasing CP coverage with increasing θ_{23} . This follows the nature of CP asymmetry that we discussed at both probability and event levels. However, once we consider the freedom of uncertainty of θ_{23} in the theory, the CP coverage drastically decreases around the maximal true value of θ_{23} in the case of DUNE. This signifies that there are CP phases in DUNE, which when considered in a fixed parameter scenario, gives a 3σ or larger sensitivity towards CPV, but they fail to attain the same when the marginalization is performed. So, these act as unfavorable CP phases in DUNE, which are absent in JD. For instance in DUNE, if we fix both data and theory at $\delta_{\text{CP}} = -148^\circ$ and $\sin^2 \theta_{23} = 0.5$, we obtain $\Delta\chi^2 = 9.82$, which drops down to 6.44 when given the freedom to $\sin^2 \theta_{23}$ to vary in the theory; however for the same set of parameters in JD, $\Delta\chi^2 = 10.6$ changes only to $\Delta\chi^2 = 10.4$ when marginalized. For this reason, in JD, the marginalization has negligible effect on the CP coverage. One of the reasons why this is dominantly visible in DUNE but not in JD, is because of the $\theta_{23} - \delta_{\text{CP}}$ degeneracy. For instance, when we generate the data with $\delta_{\text{CP}} = -145^\circ$ and $\sin^2 \theta_{23} = 0.48$ (LO), the fit chooses $\sin^2 \theta_{23} = 0.531$ (HO) in DUNE, while in JD, the fit always chooses θ_{23} from the same octant as in data. This degeneracy, as previously discussed, is indeed important when the matter potential is considerable (like in DUNE), while the same degeneracy almost vanishes when we are in a vacuum-like scenario.

Now, the dashed curves represent the contribution from only appearance, which is quite less in DUNE when compared with the CP coverage from both appearance and disappearance (solid red). However, solid and dashed blue colored curves are almost overlapping. This signifies that the disappearance effect is much more crucial in DUNE than in JD. This is because, in JD the absence of any significant matter effect reduces drastically the impact of the $\theta_{23} - \delta_{\text{CP}}$ degeneracy. Since the leading term in the disappearance channel is dependent on $\sin^2 2\theta_{23}$, it strongly constrains the θ_{23} parameter in a δ_{CP} independent manner for regions far from maximal mixing. So, the appearance channel suffers less from the $\theta_{23} - \delta_{\text{CP}}$ degeneracy for these values of $\sin^2 \theta_{23}$ in DUNE as well. However, for $\sin^2 \theta_{23}$ around MM, as discussed in Fig 3, extrinsic or matter-induced fake CP asymmetry crawls in because of the substantial matter effect in DUNE. This worsens the CP coverage, since the effect of $\theta_{23} - \delta_{\text{CP}}$ degeneracy is much more dominant. On the other hand, JD remains almost independent of this fake CP asymmetry as the matter effect is negligible here. Therefore, we must notice that despite the bigger systematic uncertainties in T2HK, it can achieve a

better CP coverage of true δ_{CP} in leptonic CPV than DUNE around the MM of $\sin^2 \theta_{23}$.

4.2 CP coverage as a function of Exposure

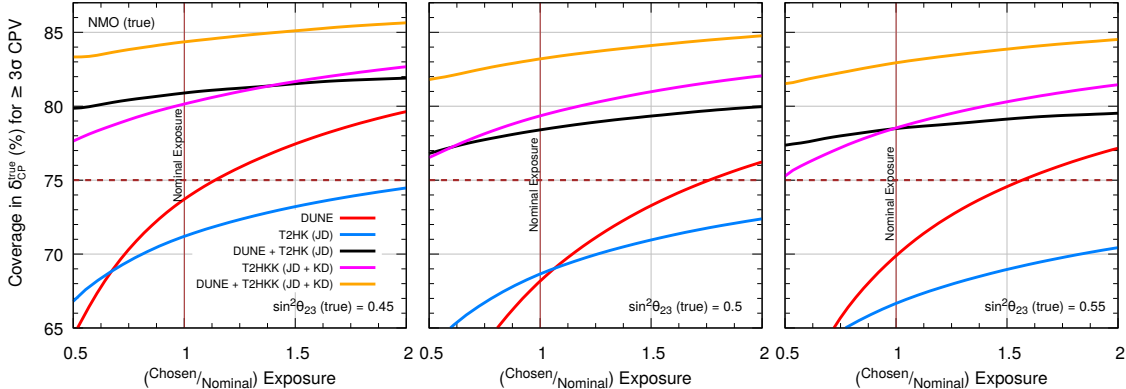


Figure 6: Coverage in true δ_{CP} for $\geq 3\sigma$ leptonic CPV as a function of scaled exposure assuming true NMO. We obtain these curves by generating the data with true $\sin^2 \theta_{23} = 0.45$ (LO), 0.5 (MM), and 0.55 (HO) and marginalizing over θ_{23} in the fit in its present 3σ range of $[0.4, 0.6]$, in the left, middle, and right panels, respectively. Here, we define scaled exposure as the ratio of assumed exposure with the nominal exposure of each experiment. Thus, (Chosen/Nominal) Exposure = 1 is the benchmark exposure of the considered setup. The curves: red, blue, black, magenta, and orange correspond to DUNE, JD, DUNE + JD, JD + KD, and DUNE + JD + KD setups, respectively.

In this section, we discuss the CP coverage of various experimental setups when total exposure in the experiment is varied. Recently, DUNE collaboration had an extensive study on how they expect to achieve desired exposure in a staged manner [20]. However, to study its effect in our analysis, we take a more simplistic approach and vary the full exposure by reducing it to half of its nominal value and increasing it to twice. In Fig. 6, we show how the CP coverage is influenced by the change in a total exposure of the experiments for $\sin^2 \theta_{23} = 0.45$ (left panel), 0.5 (middle panel), and 0.55 (right panel). The curves are shown for DUNE (red), JD (blue), DUNE + JD (black), JD + KD (magenta), and DUNE + JD + KD (orange). We obtain these by marginalizing the atmospheric angle. We observe that by keeping the true value for $\sin^2 \theta_{23}$ fixed in LO and doubling the exposure from the nominal value of 2431 (480) kt·MW·yrs in JD (DUNE), the coverage increases from 74% to 79% in DUNE and from 71% to 75% in JD. On the other hand, if the exposure is reduced up to half the nominal value, the CP coverage drastically reduces for both experiments. Also, DUNE outperforms JD when we compare both the experiments at their 70% of nominal exposures. Even though going from LO to MM, we observe a similar trend of increasing CP coverage with exposure, the maximum reachable coverage is now reduced (76% for DUNE, 72% for JD). Moreover at MM and nominal exposures, JD outperforms DUNE. This happens due to strong $\theta_{23} - \delta_{\text{CP}}$ degeneracy in DUNE near MM, which results in the reduction of CP coverage as compared to JD. In the HO case, coverage

worsens further for JD (maximum coverage 70%), but not for DUNE, which now suffers less from the $\theta_{23} - \delta_{\text{CP}}$ degeneracy under the non-maximal case. Following the previous discussion, on fixing the value of $\sin^2 \theta_{23}$, DUNE's performance improves considerably in MM, but only a little in the HO scenario.

It is interesting to note that the complementarity between DUNE and T2HK (JD) can achieve more than 75% coverage even if we consider only half of their individual nominal exposures in the three panels. As discussed earlier, JD + KD further increases the CP coverage significantly, for all the three values of true $\sin^2 \theta_{23}$. Moreover, under the nominal exposure, the combination of DUNE + JD + KD establishes CP coverage always above $\sim 80\%$.

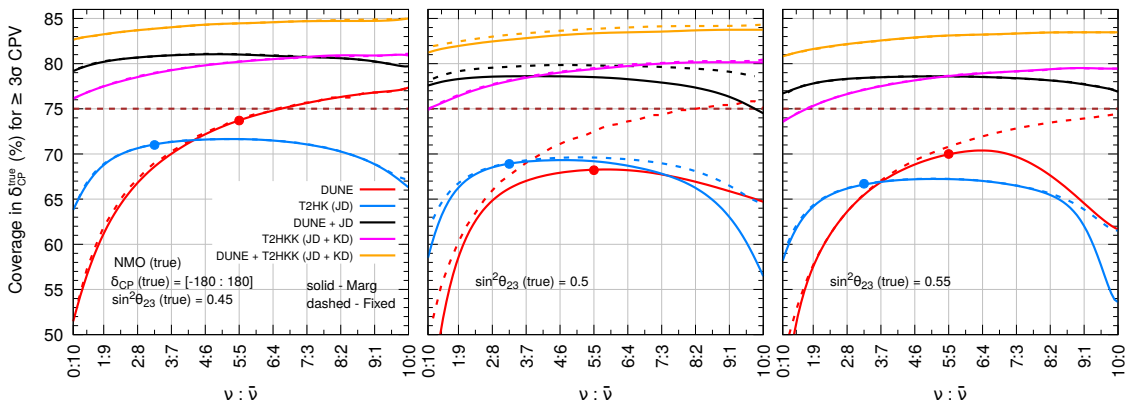


Figure 7: Coverage in true δ_{CP} for $\geq 3\sigma$ leptonic CPV as a function of the ratio of the runtime in neutrino and antineutrino ($\nu : \bar{\nu}$) modes. The left, middle, and right panels represent CP coverage with true $\sin^2 \theta_{23} = 0.45$ (LO), 0.5 (MM), and 0.55 (HO), respectively. The dashed lines are obtained by considering identical $\sin^2 \theta_{23}$ in both data and theory, while the solid lines show the result when marginalized over the present 3σ uncertain range of θ_{23} $[0.4, 0.6]$ in the theory. The curves: red, blue, black, magenta, and orange correspond to DUNE, JD, DUNE + JD, JD + KD, and DUNE + JD + KD setups, respectively. The red and blue filled circles depict the nominal runtime in DUNE $[5 \nu \text{ yrs} + 5 \bar{\nu} \text{ yrs}]$ and T2HK $[2.5 \nu \text{ yrs} + 7.5 \bar{\nu} \text{ yrs}]$, respectively. We assume true NMO in both data and fit.

4.3 Optimizing Runtime for maximal CP coverage

While discussing the total exposure, it is also important to determine the optimal runtime in neutrino and in antineutrino modes for higher CP coverage. The two collaborations have proposed different approaches. With the intent of having a similar number of neutrino and antineutrino events (see in Table 3), the T2HK (JD) plans to split the total exposure of 10 years into 2.5 years in neutrino and 7.5 years in antineutrino mode (refer to blue filled circles in Fig. 7). This choice ensures very small integrated asymmetries in the CP-conserving cases which help in highlighting easily the differences from the intrinsic asymmetries. Moreover, this choice has already been proven to be very useful for resolving degeneracies [54]. Contrastingly in DUNE, they propose a balanced ratio of runtime in neutrino and antineu-

trino modes of $[5 \nu \text{ yrs} + 5 \bar{\nu} \text{ yrs}]$ (refer to red filled circles in Fig. 7). However, this will reduce the number of events in antineutrino mode considerably but simultaneously improve the potential for the increased number of neutrino events. To visualize the discussion in Fig. 7, we represent how the ratio between neutrino and antineutrino runtime affects the coverage for all the considered setups and the usual three choices of $\sin^2 \theta_{23}$ (true) (LO, MM, and HO). We distinctly show two possible scenarios: first by fixing the same set of oscillation parameters in both data and theory (dashed curves) and second by marginalizing $\sin^2 \theta_{23}$ (solid curves) in the theory and fixing all other parameters to the benchmark choices from Table 1. In the LO case, while the nominal choice for JD $[2.5 \nu \text{ yrs} + 7.5 \bar{\nu} \text{ yrs}]$ turns out to be the best, DUNE has no advantage of running in antineutrino mode. Instead, we observe that the best coverage (77%) for DUNE is acquired when only neutrino mode is employed for the full 10 years of runtime. This is because of the δ_{CP} independent measurement of $\sin^2 \theta_{23}$ by the disappearance channel in LO. Once the atmospheric angle is constrained by disappearance, the appearance channel benefits more from the increment in statistics by running only in neutrino mode for 10 years instead of a balanced number of neutrino and antineutrino events because of the small appearance systematic uncertainties in DUNE (2%). In the maximal mixing case, the JD remains almost the same; in contrast to DUNE which establishes the best coverage for the balanced runtime scenario. This is because here the subdued abilities of the disappearance channel in the marginalized θ_{23} scenario are overcome by the balanced runtime of $[5 \nu \text{ yrs} + 5 \bar{\nu} \text{ yrs}]$, thus achieving the best coverage of 68%. While the HO case is intermediate: the best coverage in DUNE is neither obtained by the balanced $[5 \nu \text{ yrs} + 5 \bar{\nu} \text{ yrs}]$ nor with the highest number of events by fully running in only neutrino mode, rather $[6.5 \nu \text{ yrs} + 3.5 \bar{\nu} \text{ yrs}]$ scenario is best. This can be understood from previous discussions. We observe that $\sin^2 \theta_{23} (\text{true}) = 0.55$ is still in the dip region (refer to solid red in Fig. 5) but not completely, thus disappearance is not able to constrain $\sin^2 \theta_{23}$ in the fit as well as it did in MM. So, we still feel the effect of the $\theta_{23} - \delta_{\text{CP}}$ degeneracy that requires contribution from both neutrino and antineutrino modes.

However, the complementarity between the two setups play a crucial role which is essentially independent of $\sin^2 \theta_{23}$ in Nature. It is quite interesting to observe that DUNE + JD makes the choices of runtime almost irrelevant in establishing coverage in true δ_{CP} for CPV with $\geq 3\sigma$ C.L. around 75% in all the three panels, given they both run in their full exposure. DUNE + T2HKK can further improve this coverage to about 80% for the three choices of θ_{23} .

4.4 Impact of Systematic Uncertainties on CP coverage

In Fig. 8, we illustrate the effect of appearance systematic uncertainties in the coverage in true δ_{CP} for determining CPV with at least 3σ C.L. when marginalized over $\sin^2 \theta_{23}$ in the fit. It is clear that the JD curve (refer to blue colored curve) has a steeper slope than the DUNE (refer to red colored curve); however, one must note that the nominal appearance systematic uncertainties in JD (5%) is more than twice than that of DUNE (2%). Recently the T2K collaboration [8] has been considering the conservative uncertainties in the appearance systematics of about 4.9%, which they further expect to improve to about 2.7%

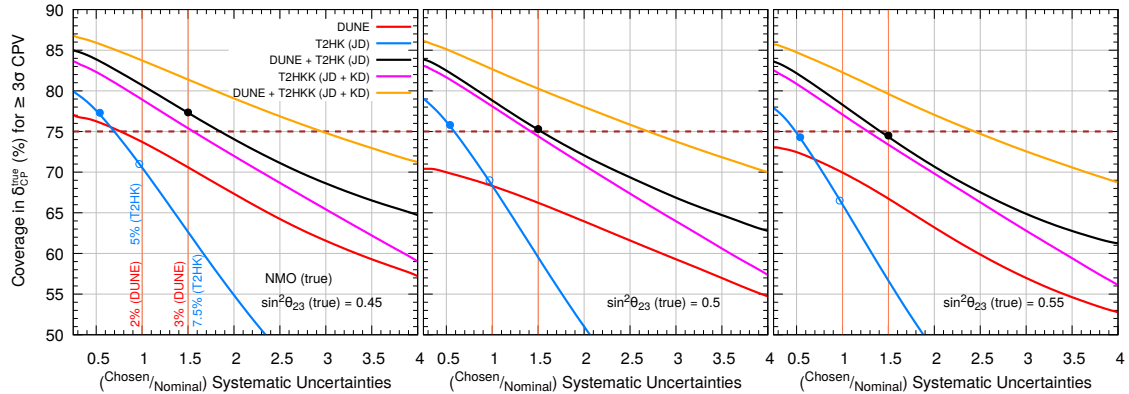


Figure 8: Coverage in true δ_{CP} for $\geq 3\sigma$ leptonic CPV as a function of scaled appearance systematic uncertainties, assuming NMO. Thus, $(\text{Chosen}/\text{Nominal})$ Systematic Uncertainties = 1 refers to the benchmark appearance systematic uncertainties (2% in DUNE and 5% in T2HK and T2HKK) of the considered experiment. In the left, middle, and right panels we obtain the results by considering true $\sin^2 \theta_{23} = 0.45$ (LO), 0.5 (MM), and 0.55 (HO), and marginalizing over the 3σ uncertain range of $\sin^2 \theta_{23}$ in the fit, respectively. The curves: red, blue, black, magenta, and orange are for DUNE, JD, DUNE + JD, JD + KD, and DUNE + JD + KD neutrino oscillation experiments, respectively. The blue colored filled and empty circles in the figure depict CP coverage corresponding to 2.7% and 4.9% systematic uncertainties in T2HK, respectively. While the black filled circles give us the coverage in true δ_{CP} for the combined DUNE + T2HK case, with each setup having 1.5 times its nominal systematic uncertainties.

by the time T2HK starts taking data [82]. Thus we also discuss these two possibilities in Fig. 8 (refer to blue empty and filled circles). Comparing the CP coverage at the expected T2HK systematics of 2.7% (filled blue circles) with the nominal in DUNE (2%), we observe that T2HK outperforms DUNE in the three possible choices of θ_{23} . We also confirm that in DUNE, the impact of the marginalization becomes negligible when systematics are higher than 5%, so the coverage in true δ_{CP} becomes completely systematics dominated.

Contrastingly, in Nature, if the real appearance systematic uncertainty turns out to be about 1.5 times higher than its nominal value in both DUNE and T2HK setups, then the complementarity between them is the only solution to achieve 75% of coverage in true δ_{CP} for the three possible choices of θ_{23} : 0.45, 0.5, and 0.55 (refer to the coordinates of black filled circles in each panel). Also, when we include the second proposed detector: KD, in the analysis along with DUNE (refer to the orange curve), we achieve the milestone of 75% coverage, even if appearance systematics is increased by a factor of 2.5 for three possible choices of true θ_{23} .

4.5 Effect of Current 3σ Allowed Range in δ_{CP} on CP coverage

In all the previous results, we use the entire allowed range of $\delta_{\text{CP}} \in [-180^\circ, 180^\circ]$ for generating data. However, the presently running LBL accelerator experiments: T2K [8] and NOvA [10] along with strong precision measurements of θ_{13} from the Daya Bay [83]

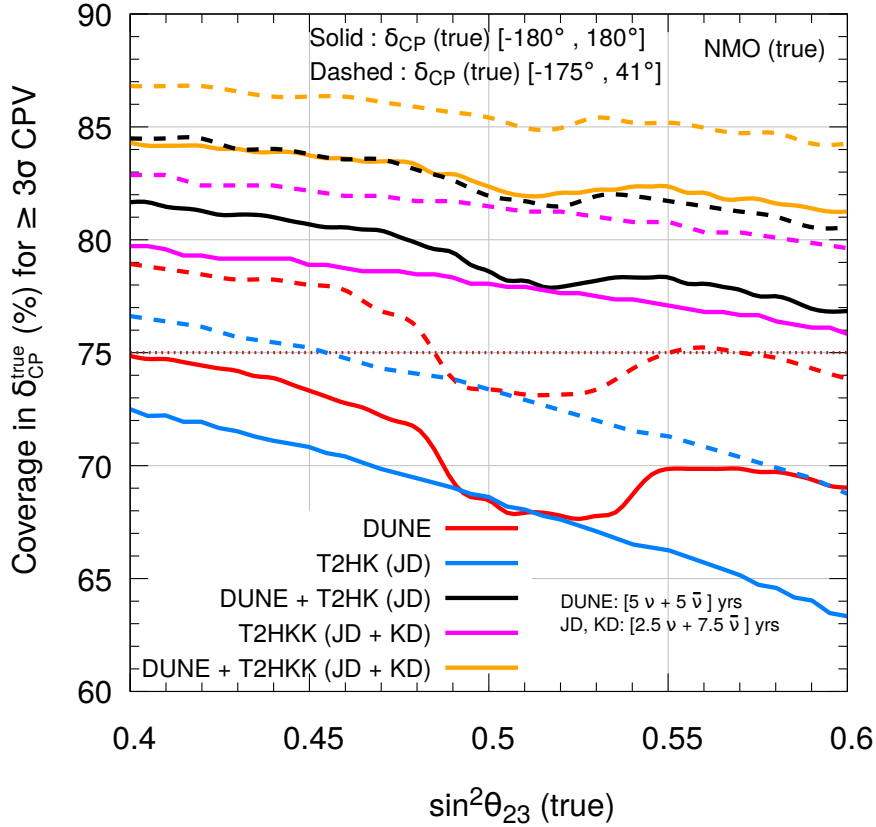


Figure 9: Coverage in true δ_{CP} for $\geq 3\sigma$ leptonic CPV as a function of $\sin^2 \theta_{23}$ (true) while marginalizing over θ_{23} in the fit. The solid curves represent the results wherein we generate data assuming the entire range of δ_{CP} (true) $\in [-180^\circ, 180^\circ]$ and exclude test $\delta_{\text{CP}} = 0^\circ$ and 180° in the fit. On the other hand, the dashed curves show the results when we generate data considering only the present 3σ allowed range of δ_{CP} (true) $\in [-175^\circ, 41^\circ]$ [7] and exclude test $\delta_{\text{CP}} = 0^\circ$ in the fit. The curves: red, blue, black, magenta, and orange are for DUNE, JD, DUNE + JD, JD + KD, and DUNE + JD + KD setups, respectively. We assume NMO in both data and theory.

has helped global oscillation data analyses [4–7] to put constraints on δ_{CP} . So, it becomes imperative to discuss the results within these bounds which might get established with better precision in the coming years.

In this subsection, we repeat some of our analysis using the present 3σ allowed range of $\delta_{\text{CP}} \in [-175^\circ, 41^\circ]$ with a relative 1σ uncertainty of 16% as obtained in Ref.[7]. Since one of the CP-conserving cases, $\delta_{\text{CP}} = 180^\circ$ is ruled out in the present 3σ bound, we now use only $\delta_{\text{CP}} = 0^\circ$ in the fit and define the Poissonian $\Delta\chi^2$ [70] following the frequentist approach [72] as follows

$$\Delta\chi^2 = \min_{(\theta_{23}, \lambda_1, \lambda_2)} \left[\chi^2(\delta_{\text{CP}}^{\text{true}} \in [-175^\circ, 41^\circ]) - \chi^2(\delta_{\text{CP}}^{\text{test}} = 0^\circ) \right]. \quad (4.2)$$

where λ_1 , and λ_2 are the pull parameters in signal and background, respectively. We calculate CP coverage for different experimental setups using Eq. 4.2. In Fig. 9, we show coverage in true δ_{CP} which can establish CPV with at least 3σ C.L. as a function of $\sin^2 \theta_{23}$. The dashed colored curves represent the CP coverage of a given setup calculated using the 3σ bounds on δ_{CP} . We observe that with better constraints on δ_{CP} , we improve the coverage in δ_{CP} consistently for each $\sin^2 \theta_{23}$ by almost (4 - 5)% in both DUNE and JD. Previously in the unconstrained scenario (red solid curve), DUNE does not attain the benchmark of 75% coverage for any value of $\sin^2 \theta_{23}$, however, with the new definition (dashed red curve) DUNE can attain 75% of CP coverage for about 58% of $\sin^2 \theta_{23}$ in Nature. Therefore, if in Nature $\sin^2 \theta_{23}$ turns out to be in any value in LO, then DUNE can easily achieve the milestone of 75% coverage with the nominal appearance systematics and exposure. Similarly, JD which previously with the entire range of δ_{CP} , could achieve only 72% of CP coverage in the most favorable zone (solid blue curve) improves further to 75% (dashed blue curve) of coverage if $\sin^2 \theta_{23} \in [0.4, 0.45]$ in Nature. As expected the combined setups can achieve enhanced coverage as well. This increment in CP coverage is quite expected as here we generate data with a more constrained bound on δ_{CP} , and also in the fit, we consider only one CP-conserving ($\delta_{\text{CP}} = 0^\circ$) value for studying CP violation.

5 Summary and Conclusions

The current knowledge of the active three-neutrino mixing angles has reached unprecedented precision. One of the remaining goals is to establish CPV in the leptonic sector. Even though hints for non-vanishing δ_{CP} are emerging from the current neutrino data, it is worth testing the capability of future long-baseline experiments to establish leptonic CPV at at least 3σ C.L. for a large set of true δ_{CP} in the whole canvas of $[-180^\circ, 180^\circ]$ range. In our study, we investigate the abilities of DUNE, T2HK (JD), and T2HKK (JD with a possible second detector in Korea, KD) to establish the CPV. We obtain the range of true δ_{CP} which establishes CPV for $\geq 3\sigma$ confidence level. The ratio of this range and the entire allowed range of δ_{CP} is termed as CP coverage. From our analyses, we conclude that none of the experiments individually can attain the desired landmark of 75% CP coverage. However, the complementarities in the combined setup of DUNE + JD, JD + KD, and DUNE + JD + KD can accomplish the goal, irrespective of the value of θ_{23} chosen by Nature. Even though JD has a relatively less matter effect and thus better access to genuine CP than DUNE, we observe that CP coverage of JD is lesser than DUNE for all values of θ_{23} . We observe that this is due to the higher nominal systematic uncertainties in the appearance channel in JD (5%) than in DUNE (2%). Thus, systematic uncertainties play a critical role in determining CP coverage. Also, we observe that if we cannot handle the larger systematic uncertainties in the future, complementarity among different setups will suffice in reaching the milestone of 75% coverage in true δ_{CP} for leptonic CPV at 3σ . We also determine quantitatively that the combined setup of DUNE + JD needs only half of their individual nominal exposures to reach the expected goal. Complementarity among combined experiments lead to an exposure independent determination of CP coverage. In fact, we show that even at the lower exposures, the CP coverage from combined setups

is way better than standalone experiments considered with much higher exposures. To

$\sin^2 \theta_{23}$	Coverage in true δ_{CP} for $\geq 3\sigma$ CPV (%)		
	DUNE	T2HK	DUNE + T2HK
0.45	73	71 (77)	81 (83)
0.5	68	69 (76)	78 (79)
0.55	70	66 (74)	79 (80)

Table 4: Coverage in true δ_{CP} for $\geq 3\sigma$ leptonic CPV with nominal exposure and appearance systematic uncertainties is determined in DUNE, T2HK (JD), and DUNE + T2HK (JD) as a function of three $\sin^2 \theta_{23}$: 0.45, 0.5, and 0.55. The data is generated by fixing all the oscillation parameters at their benchmark values from Table 1 and varying CP phase in the entire range of $[-180^\circ, 180^\circ]$, while the fit is marginalized over the 3σ range in θ_{23} assuming true NMO. The values in the parenthesis have been generated by considering an improved appearance systematic uncertainty of 2.7% in T2HK instead of the nominal value of 5%.

summarize, we estimate the percentage of CP coverage achievable by DUNE, T2HK, and DUNE + T2HK considering the nominal exposures and appearance systematic uncertainties in DUNE (2%) and T2HK (5%) in Table 4. It is quite vivid how complementarity between DUNE and T2HK, increases CP coverage in the most unfavorable zone in DUNE (T2HK) by about 10% (13%). The bracketed value gives coverage in true δ_{CP} for leptonic CPV with at least 3σ C.L. when a reduced 2.7% appearance systematic uncertainties are considered in T2HK. It is quite interesting to observe how improved systematics exhibit a significant increment in the CP coverage in three probable choices of θ_{23} and makes T2HK individually capable to establish CPV with at least 3σ C.L. for about 80% of CP phases. While the combined setup does not exhibit much improvement. This is because in T2HK there is no $\theta_{23} - \delta_{\text{CP}}$ degeneracy, thus by reducing the uncertainties in systematics we improve the coverage. While in the combined setup, the $\theta_{23} - \delta_{\text{CP}}$ degeneracy in DUNE does not allow much improvement in coverage even with the reduced systematic uncertainties in T2HK.

Regarding runtime, we observe that:

- if in Nature, θ_{23} turns out to be in LO ($\sin^2 \theta_{23} = 0.45$), then DUNE does not need run in $\bar{\nu}$ mode, as CP coverage then simply becomes proportional to ν statistics;
- if in Nature, θ_{23} turns out to be MM or HO ($\sin^2 \theta_{23} = 0.55$), run in $\bar{\nu}$ mode helps in overcoming the $\theta_{23} - \delta_{\text{CP}}$ degeneracy;
- in T2HK, a balanced run is better for establishing better coverage in true δ_{CP} ;
- the complementarity among different setups surpasses the need of running in $\bar{\nu}$ mode in either of the three probable choices of θ_{23} .

We also explore the percentage in true δ_{CP} for $\geq 3\sigma$ leptonic CPV, if we generate the data with the current 3σ bounds of δ_{CP} . This improves the CP coverage by (5 - 6)% in both DUNE and T2HK consistently for all values of θ_{23} . With the present 3σ bounds on

δ_{CP} , DUNE can achieve 75% of CP coverage in true δ_{CP} for about 58% of θ_{23} in Nature. Also, if $\theta_{23} \in [40^\circ, 45^\circ]$ in Nature, then JD can also achieve the landmark coverage in true δ_{CP} with the nominal appearance systematics and exposure. As a final remark, we also discuss the importance of having the disappearance channel in our analysis of the CPV sensitivity. Although being independent of intrinsic CP asymmetry, disappearance helps in constraining θ_{23} and thus reduces the $\theta_{23} - \delta_{\text{CP}}$ degeneracy that is primarily responsible for lowering the CP coverage in δ_{CP} .

Acknowledgments

S.K.A would like to thank the conveners of the Neutrino Physics Frontier for providing him an opportunity to present the preliminary results from this work in the Snowmass Community Summer Study Workshop at the University of Washington, Seattle, USA during 17th to 26th July, 2022. S.K.A and S.D. acknowledge the support from the Department of Atomic Energy (DAE), Govt. of India, under the Project Identification Number RIO 4001. S.K.A. is supported by the Young Scientist Research Grant [INSA/SP/YSP/144/2017/1578] from the Indian National Science Academy (INSA). S.K.A. acknowledges the financial support from the Swarnajayanti Fellowship (sanction order No. DST/SJF/PSA- 05/2019-20) provided by the Department of Science and Technology (DST), Govt. of India, and the Research Grant (sanction order No. SB/SJF/2020-21/21) provided by the Science and Engineering Research Board (SERB), Govt. of India, under the Swarnajayanti Fellowship project. S.K.A would like to thank the United States-India Educational Foundation for providing the financial support through the Fulbright-Nehru Academic and Professional Excellence Fellowship (Award No. 2710/F-N APE/2021). M.S. acknowledges financial support from the DST, Govt. of India (DST/INSPIRE Fellowship/2018/IF180059). The numerical simulations are carried out using the ‘‘SAMKHYA: High-Performance Computing Facility’’ at Institute of Physics, Bhubaneswar, India.

References

- [1] A. D. Sakharov, *Violation of CP Invariance, C asymmetry, and baryon asymmetry of the universe*, *Pisma Zh. Eksp. Teor. Fiz.* **5** (1967) 32–35.
- [2] **Particle Data Group** Collaboration, R. L. Workman et al., *Review of Particle Physics*, *PTEP* **2022** (2022) 083C01.
- [3] **Daya Bay** Collaboration, F. P. An et al., *Observation of electron-antineutrino disappearance at Daya Bay*, *Phys. Rev. Lett.* **108** (2012) 171803, [[arXiv:1203.1669](#)].
- [4] P. F. de Salas, D. V. Forero, S. Gariazzo, P. Martínez-Miravé, O. Mena, C. A. Ternes, M. Tórtola, and J. W. F. Valle, *2020 global reassessment of the neutrino oscillation picture*, *JHEP* **02** (2021) 071, [[arXiv:2006.11237](#)].
- [5] I. Esteban, M. C. Gonzalez-Garcia, M. Maltoni, T. Schwetz, and A. Zhou, *The fate of hints: updated global analysis of three-flavor neutrino oscillations*, *JHEP* **09** (2020) 178, [[arXiv:2007.14792](#)].
- [6] NuFIT v5.1 (2021), <http://www.nu-fit.org/>.

- [7] F. Capozzi, E. Di Valentino, E. Lisi, A. Marrone, A. Melchiorri, and A. Palazzo, *Unfinished fabric of the three neutrino paradigm*, *Phys. Rev. D* **104** (2021), no. 8 083031, [[arXiv:2107.00532](#)].
- [8] **T2K** Collaboration, K. Abe et al., *Constraint on the matter–antimatter symmetry-violating phase in neutrino oscillations*, *Nature* **580** (2020), no. 7803 339–344, [[arXiv:1910.03887](#)]. [Erratum: *Nature* 583, E16 (2020)].
- [9] **T2K** Collaboration, K. Abe et al., *Improved constraints on neutrino mixing from the T2K experiment with 3.13×10^{21} protons on target*, *Phys. Rev. D* **103** (2021), no. 11 112008, [[arXiv:2101.03779](#)].
- [10] **NOvA** Collaboration, M. A. Acero et al., *An Improved Measurement of Neutrino Oscillation Parameters by the NOvA Experiment*, [arXiv:2108.08219](#).
- [11] S. Pascoli, S. T. Petcov, and A. Riotto, *Connecting low energy leptonic CP-violation to leptogenesis*, *Phys. Rev. D* **75** (2007) 083511, [[hep-ph/0609125](#)].
- [12] G. C. Branco, R. G. Felipe, and F. R. Joaquim, *Leptonic CP Violation*, *Rev. Mod. Phys.* **84** (2012) 515–565, [[arXiv:1111.5332](#)].
- [13] S. T. Petcov, *Predicting the values of the leptonic CP violation phases in theories with discrete flavour symmetries*, *Nucl. Phys. B* **892** (2015) 400–428, [[arXiv:1405.6006](#)].
- [14] C. Hagedorn, R. N. Mohapatra, E. Molinaro, C. C. Nishi, and S. T. Petcov, *CP Violation in the Lepton Sector and Implications for Leptogenesis*, *Int. J. Mod. Phys. A* **33** (2018), no. 05n06 1842006, [[arXiv:1711.02866](#)].
- [15] **DUNE** Collaboration, R. Acciarri et al., *Long-Baseline Neutrino Facility (LBNF) and Deep Underground Neutrino Experiment (DUNE): Conceptual Design Report, Volume 2: The Physics Program for DUNE at LBNF*, [arXiv:1512.06148](#).
- [16] **DUNE** Collaboration, B. Abi et al., *Deep Underground Neutrino Experiment (DUNE), Far Detector Technical Design Report, Volume I Introduction to DUNE*, *JINST* **15** (2020), no. 08 T08008, [[arXiv:2002.02967](#)].
- [17] **DUNE** Collaboration, B. Abi et al., *Deep Underground Neutrino Experiment (DUNE), Far Detector Technical Design Report, Volume II: DUNE Physics*, [arXiv:2002.03005](#).
- [18] **DUNE** Collaboration, B. Abi et al., *Long-baseline neutrino oscillation physics potential of the DUNE experiment*, *Eur. Phys. J. C* **80** (2020), no. 10 978, [[arXiv:2006.16043](#)].
- [19] **DUNE** Collaboration, B. Abi et al., *Experiment Simulation Configurations Approximating DUNE TDR*, [arXiv:2103.04797](#).
- [20] **DUNE** Collaboration, A. A. Abud et al., *Low exposure long-baseline neutrino oscillation sensitivity of the DUNE experiment*, [arXiv:2109.01304](#).
- [21] **Hyper-Kamiokande Proto-** Collaboration, K. Abe et al., *Physics potential of a long-baseline neutrino oscillation experiment using a J-PARC neutrino beam and Hyper-Kamiokande*, *PTEP* **2015** (2015) 053C02, [[arXiv:1502.05199](#)].
- [22] **Hyper-Kamiokande** Collaboration, K. Abe et al., *Hyper-Kamiokande Design Report*, [arXiv:1805.04163](#).
- [23] **Hyper-Kamiokande** Collaboration, K. Abe et al., *Physics potentials with the second Hyper-Kamiokande detector in Korea*, *PTEP* **2018** (2018), no. 6 063C01, [[arXiv:1611.06118](#)].

- [24] S. Fukasawa, M. Ghosh, and O. Yasuda, *Complementarity Between Hyperkamiokande and DUNE in Determining Neutrino Oscillation Parameters*, *Nucl. Phys. B* **918** (2017) 337–357, [[arXiv:1607.03758](#)].
- [25] P. Ballett, S. F. King, S. Pascoli, N. W. Prouse, and T. Wang, *Sensitivities and synergies of DUNE and T2HK*, *Phys. Rev. D* **96** (2017), no. 3 033003, [[arXiv:1612.07275](#)].
- [26] J. Liao, D. Marfatia, and K. Whisnant, *Nonstandard neutrino interactions at DUNE, T2HK and T2HKK*, *JHEP* **01** (2017) 071, [[arXiv:1612.01443](#)].
- [27] M. Ghosh and O. Yasuda, *Effect of systematics in the T2HK, T2HKK, and DUNE experiments*, *Phys. Rev. D* **96** (2017), no. 1 013001, [[arXiv:1702.06482](#)].
- [28] S. Choubey, D. Dutta, and D. Pramanik, *Imprints of a light Sterile Neutrino at DUNE, T2HK and T2HKK*, *Phys. Rev. D* **96** (2017), no. 5 056026, [[arXiv:1704.07269](#)].
- [29] S. K. Agarwalla, S. Das, A. Giarnetti, and D. Meloni, *Model-Independent Constraints on Non-Unitary Neutrino Mixing from High-Precision Long-Baseline Experiments*, [[arXiv:2111.00329](#)].
- [30] S. K. Agarwalla, S. Prakash, and S. Uma Sankar, *Exploring the three flavor effects with future superbeams using liquid argon detectors*, *JHEP* **03** (2014) 087, [[arXiv:1304.3251](#)].
- [31] N. Nath, M. Ghosh, and S. Goswami, *The physics of antineutrinos in DUNE and determination of octant and δ_{CP}* , *Nucl. Phys. B* **913** (2016) 381–404, [[arXiv:1511.07496](#)].
- [32] P. A. N. Machado, *Learning about the CP phase in the next 10 years*, *Nucl. Part. Phys. Proc.* **265-266** (2015) 174–176, [[arXiv:1503.03775](#)].
- [33] **Particle Data Group** Collaboration, P. Zyla et al., *Review of Particle Physics*, *PTEP* **2020** (2020), no. 8 083C01.
- [34] S. K. Agarwalla, R. Kundu, S. Prakash, and M. Singh, *A close look on 2-3 mixing angle with DUNE in light of current neutrino oscillation data*, *JHEP* **03** (2022) 206, [[arXiv:2111.11748](#)].
- [35] E. K. Akhmedov, R. Johansson, M. Lindner, T. Ohlsson, and T. Schwetz, *Series expansions for three flavor neutrino oscillation probabilities in matter*, *JHEP* **04** (2004) 078, [[hep-ph/0402175](#)].
- [36] B. Roe, *Matter density versus distance for the neutrino beam from Fermilab to Lead, South Dakota, and comparison of oscillations with variable and constant density*, *Phys. Rev. D* **95** (2017), no. 11 113004, [[arXiv:1707.02322](#)].
- [37] G. L. Fogli and E. Lisi, *Tests of three-flavor mixing in long-baseline neutrino oscillation experiments*, *Phys. Rev.* **D54** (1996) 3667–3670, [[hep-ph/9604415](#)].
- [38] V. Barger, D. Marfatia, and K. Whisnant, *Breaking eight fold degeneracies in neutrino CP violation, mixing, and mass hierarchy*, *Phys. Rev. D* **65** (2002) 073023, [[hep-ph/0112119](#)].
- [39] H. Minakata, H. Nunokawa, and S. J. Parke, *Parameter Degeneracies in Neutrino Oscillation Measurement of Leptonic CP and T Violation*, *Phys. Rev. D* **66** (2002) 093012, [[hep-ph/0208163](#)].
- [40] H. Minakata, M. Sonoyama, and H. Sugiyama, *Determination of θ_{23} in long-baseline neutrino oscillation experiments with three-flavor mixing effects*, *Phys. Rev. D* **70** (2004) 113012, [[hep-ph/0406073](#)].

- [41] K. Hiraide, H. Minakata, T. Nakaya, H. Nunokawa, H. Sugiyama, W. J. C. Teves, and R. Z. Funchal, *Resolving θ_{23} degeneracy by accelerator and reactor neutrino oscillation experiments*, *Phys. Rev. D* **73** (2006) 093008, [[hep-ph/0601258](#)].
- [42] C. R. Das, J. a. Pulido, J. Maalampi, and S. Vihonen, *Determination of the θ_{23} octant in long baseline neutrino experiments within and beyond the standard model*, *Phys. Rev. D* **97** (2018), no. 3 035023, [[arXiv:1708.05182](#)].
- [43] M. Tanimoto, *Indirect search for CP violation in neutrino oscillations*, *Phys. Lett. B* **435** (1998) 373–380, [[hep-ph/9806375](#)].
- [44] V. D. Barger, K. Whisnant, S. Pakvasa, and R. J. N. Phillips, *Matter Effects on Three-Neutrino Oscillations*, *Phys. Rev. D* **22** (1980) 2718.
- [45] J. Arafune, M. Koike, and J. Sato, *CP violation and matter effect in long baseline neutrino oscillation experiments*, *Phys. Rev. D* **56** (1997) 3093–3099, [[hep-ph/9703351](#)]. [Erratum: *Phys.Rev.D* 60, 119905 (1999)].
- [46] J. Bernabéu and A. Segarra, *Do T asymmetries for neutrino oscillations in uniform matter have a CP-even component?*, *JHEP* **03** (2019) 103, [[arXiv:1901.02761](#)].
- [47] J. Bernabéu and A. Segarra, *Signatures of the genuine and matter-induced components of the CP violation asymmetry in neutrino oscillations*, *JHEP* **11** (2018) 063, [[arXiv:1807.11879](#)].
- [48] T. Ohlsson and S. Zhou, *Extrinsic and Intrinsic CPT Asymmetries in Neutrino Oscillations*, *Nucl. Phys. B* **893** (2015) 482–500, [[arXiv:1408.4722](#)].
- [49] H. Nunokawa, S. J. Parke, and J. W. F. Valle, *CP Violation and Neutrino Oscillations*, *Prog. Part. Nucl. Phys.* **60** (2008) 338–402, [[arXiv:0710.0554](#)].
- [50] A. Giarnetti and D. Meloni, *New Sources of Leptonic CP Violation at the DUNE Neutrino Experiment*, *Universe* **7** (2021), no. 7 240, [[arXiv:2106.00030](#)].
- [51] J. Rout, S. Shafaq, M. Bishai, and P. Mehta, *Physics prospects with the second oscillation maximum at the Deep Underground Neutrino Experiment*, *Phys. Rev. D* **103** (2021), no. 11 116003, [[arXiv:2012.08269](#)].
- [52] M. Blennow, E. Fernandez-Martinez, T. Ota, and S. Rosauero-Alcaraz, *Physics potential of the ESS ν SB*, *Eur. Phys. J. C* **80** (2020), no. 3 190, [[arXiv:1912.04309](#)].
- [53] J. Tang, S. Vihonen, and T.-C. Wang, *Precision measurements on δ_{CP} in MOMENT*, *JHEP* **12** (2019) 130, [[arXiv:1909.01548](#)].
- [54] S. K. Agarwalla, S. Prakash, and S. U. Sankar, *Resolving the octant of θ_{23} with T2K and NO ν A*, *JHEP* **07** (2013) 131, [[arXiv:1301.2574](#)].
- [55] H. Minakata and S. J. Parke, *Correlated, precision measurements of θ_{23} and δ using only the electron neutrino appearance experiments*, *Phys. Rev. D* **87** (2013), no. 11 113005, [[arXiv:1303.6178](#)].
- [56] P. Coloma, A. Donini, E. Fernandez-Martinez, and P. Hernandez, *Precision on leptonic mixing parameters at future neutrino oscillation experiments*, *JHEP* **06** (2012) 073, [[arXiv:1203.5651](#)].
- [57] **Hyper-Kamiokande** Collaboration, K. Abe et al., *Hyper-Kamiokande Design Report*, [[arXiv:1805.04163](#)].
- [58] G. J. Feldman, J. Hartnell, and T. Kobayashi, *Long-baseline neutrino oscillation experiments*, *Advances in High Energy Physics* **2013** (2013) 1–30.

- [59] S. K. Agarwalla, *Physics Potential of Long-Baseline Experiments*, *Adv. High Energy Phys.* **2014** (2014) 457803, [[arXiv:1401.4705](#)].
- [60] M. Diwan, V. Galymov, X. Qian, and A. Rubbia, *Long-baseline neutrino experiments*, *Annual Review of Nuclear and Particle Science* **66** (oct, 2016) 47–71.
- [61] C. Giganti, S. Lavignac, and M. Zito, *Neutrino oscillations: The rise of the PMNS paradigm*, *Prog. Part. Nucl. Phys.* **98** (2018) 1–54, [[arXiv:1710.00715](#)].
- [62] **OPERA** Collaboration, N. Agafonova et al., *Final Results of the OPERA Experiment on ν_τ Appearance in the CNGS Neutrino Beam*, *Phys. Rev. Lett.* **120** (2018), no. 21 211801, [[arXiv:1804.04912](#)]. [Erratum: *Phys.Rev.Lett.* 121, 139901 (2018)].
- [63] A. De Gouvêa, K. J. Kelly, G. V. Stenico, and P. Pasquini, *Physics with Beam Tau-Neutrino Appearance at DUNE*, *Phys. Rev. D* **100** (2019), no. 1 016004, [[arXiv:1904.07265](#)].
- [64] A. Ghoshal, A. Giarnetti, and D. Meloni, *On the role of the ν_τ appearance in DUNE in constraining standard neutrino physics and beyond*, *JHEP* **12** (2019) 126, [[arXiv:1906.06212](#)].
- [65] R. Mammen Abraham et al., *Tau neutrinos in the next decade: from GeV to EeV*, *J. Phys. G* **49** (2022), no. 11 110501, [[arXiv:2203.05591](#)].
- [66] P. Huber and W. Winter, *Neutrino factories and the ‘magic’ baseline*, *Phys. Rev. D* **68** (2003) 037301, [[hep-ph/0301257](#)].
- [67] A. Donini, D. Meloni, and S. Rigolin, *Clone flow analysis for a theory inspired neutrino experiment planning*, *JHEP* **06** (2004) 011, [[hep-ph/0312072](#)].
- [68] S. K. Agarwalla, *Some Aspects of Neutrino Mixing and Oscillations*. PhD thesis, Calcutta U., 2008. [arXiv:0908.4267](#).
- [69] P. Machado, H. Schulz, and J. Turner, *Tau neutrinos at DUNE: New strategies, new opportunities*, *Phys. Rev. D* **102** (2020), no. 5 053010, [[arXiv:2007.00015](#)].
- [70] S. Baker and R. D. Cousins, *Clarification of the Use of Chi Square and Likelihood Functions in Fits to Histograms*, *Nucl. Instrum. Meth.* **221** (1984) 437–442.
- [71] G. Cowan, K. Cranmer, E. Gross, and O. Vitells, *Asymptotic formulae for likelihood-based tests of new physics*, *Eur. Phys. J. C* **71** (2011) 1554, [[arXiv:1007.1727](#)]. [Erratum: *Eur.Phys.J.C* 73, 2501 (2013)].
- [72] M. Blennow, P. Coloma, P. Huber, and T. Schwetz, *Quantifying the sensitivity of oscillation experiments to the neutrino mass ordering*, *JHEP* **03** (2014) 028, [[arXiv:1311.1822](#)].
- [73] P. Huber, M. Lindner, and W. Winter, *Superbeams versus neutrino factories*, *Nucl. Phys. B* **645** (2002) 3–48, [[hep-ph/0204352](#)].
- [74] G. L. Fogli, E. Lisi, A. Marrone, D. Montanino, and A. Palazzo, *Getting the most from the statistical analysis of solar neutrino oscillations*, *Phys. Rev. D* **66** (2002) 053010, [[hep-ph/0206162](#)].
- [75] M. C. Gonzalez-Garcia and M. Maltoni, *Atmospheric neutrino oscillations and new physics*, *Phys. Rev. D* **70** (2004) 033010, [[hep-ph/0404085](#)].
- [76] A. M. Ankowski and C. Mariani, *Systematic uncertainties in long-baseline neutrino-oscillation experiments*, *J. Phys. G* **44** (2017), no. 5 054001, [[arXiv:1609.00258](#)].
- [77] **JUNO** Collaboration, A. Abusleme et al., *Sub-percent Precision Measurement of Neutrino Oscillation Parameters with JUNO*, [arXiv:2204.13249](#).

- [78] **Super-Kamiokande** Collaboration, P. Fernandez Menendez, *Atmospheric neutrino oscillations with Super-Kamiokande and prospects for SuperK-Gd*, *PoS ICRC2021* (2021) 008.
- [79] **IceCube** Collaboration, K. Leonard DeHolton, *Atmospheric Neutrino Oscillations with 8 years of data from IceCube DeepCore*, *PoS NuFact2021* (2022) 062.
- [80] P. Huber, M. Lindner, and W. Winter, *Simulation of long-baseline neutrino oscillation experiments with GLOBES (General Long Baseline Experiment Simulator)*, *Comput. Phys. Commun.* **167** (2005) 195, [[hep-ph/0407333](#)].
- [81] P. Huber, J. Kopp, M. Lindner, M. Rolinec, and W. Winter, *New features in the simulation of neutrino oscillation experiments with GLOBES 3.0: General Long Baseline Experiment Simulator*, *Comput. Phys. Commun.* **177** (2007) 432–438, [[hep-ph/0701187](#)].
- [82] L.-I. Munteanu, *Long-baseline neutrino oscillation sensitivities with Hyper-Kamiokande*, *PoS NuFact2021* (2022) 056.
- [83] K.-B. Luk, *Reactor Neutrino: Latest Results from Daya Bay*, *Neutrino2022*, .